USGS
science for a changing world

Prepared in cooperation with the U.S. Army Corps of Engineers

Geophysical Investigations at Hidden Dam, Raymond, California—Flow Simulations

By Burke J. Minsley and Scott Ikard

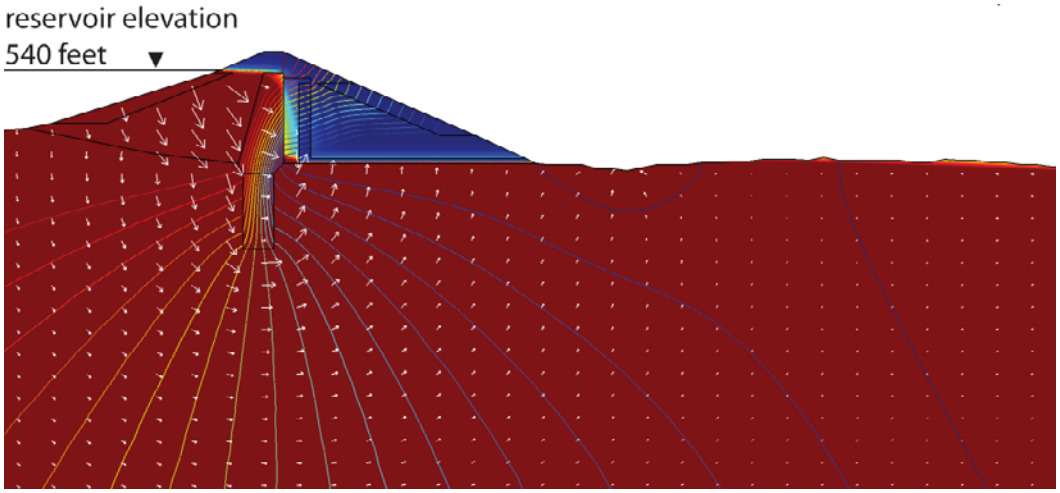

Open-File Report 2010–1153

U.S. Department of the Interior
U.S. Geological Survey

U.S. Department of the Interior
KEN SALAZAR, Secretary

U.S. Geological Survey
Marcia K. McNutt, Director

U.S. Geological Survey, Reston, Virginia: 2010

For product and ordering information:
World Wide Web: http://www.usgs.gov/pubprod
Telephone: 1-888-ASK-USGS

For more information on the USGS—the Federal source for science about the Earth,
its natural and living resources, natural hazards, and the environment:
World Wide Web: http://www.usgs.gov
Telephone: 1-888-ASK-USGS

Suggested citation:
Minsley, B.J., and Ikard, Scott, 2010, Geophysical investigations at Hidden Dam, Raymond, California—Flow simulations: U.S. Geological Survey Open-File Report 2010–1153, 64 p.

Contents

Figures

Tables

Conversion Factors

Inch/Pound to SI

Multiply	By	To obtain
	Length	
inch (in.)	2.54	centimeter (cm)
foot (ft)	0.3048	meter (m)
mile (mi)	1.609	kilometer (km)
	Area	
acre	4,047	square meter (m^2)
acre	0.004047	square kilometer (km^2)
square mile (mi^2)	2.590	square kilometer (km^2)
	Volume	
gallon (gal)	0.003785	cubic meter (m^3)
acre-foot (acre-ft)	1,233	cubic meter (m^3)
	Flow rate	
foot per day (ft/d)	0.3048	meter per day (m/d)
cubic foot per day (ft^3/d)	0.02832	cubic meter per day (m^3/d)
gallon per minute (gal/min)	0.06309	liter per second (L/s)
gallon per day (gal/d)	0.003785	cubic meter per day (m^3/d)
	Mass	
pound, avoirdupois (lb)	0.4536	kilogram (kg)
	Pressure	
pound-force per square foot (lb/ft^2)	0.04788	kilopascal (kPa)
	Density	
pound per cubic foot (lb/ft^3)	16.02	kilogram per cubic meter (kg/m^3)
	Acceleration	
foot per square second (ft/s^2)	0.3048	meter per square second (m/s^2)
	Hydraulic conductivity	
foot per day (ft/d)	0.3048	meter per day (m/d)

Vertical coordinate information is referenced to North American Vertical Datum of 1988 (NAVD 88).

Horizontal coordinate information is referenced to the North American Datum of 1983 (NAD 83).

Elevation, as used in this report, refers to distance above the vertical datum.

Electrical Conductivity and Electrical Resistivity

Multiply	By	To obtain
	Electrical conductivity	
siemens per meter (S/m)	1,000	millisiemens per meter (mS/m)
siemens per meter (S/m)	10,000	microsiemens per meter (μS/cm)
	Electrical resistivity	
ohm-meters (ohm-m)	0.001	kiloohm-meters (kohm-m)

Electrical conductivity σ in siemens per meter (S/m) can be converted to electrical resistivity ρ in ohm-meters (ohm-m) as follows: $\rho = 1/\sigma$.

Electrical resistivity ρ in ohm-meters (ohm-m) can be converted to electrical conductivity σ in siemens per meter (S/m) as follows: $\sigma = 1/\rho$.

Geophysical Investigations at Hidden Dam, Raymond, California—Flow Simulations

By Burke J. Minsley and Scott Ikard

Introduction

Numerical flow modeling and analysis of observation-well data at Hidden Dam are carried out to supplement recent geophysical field investigations at the site (Minsley and others, 2010). This work also is complementary to earlier seepage-related studies at Hidden Dam documented by Cedergren (1980a, b). Known seepage areas on the northwest right abutment area of the downstream side of the dam was documented by Cedergren (1980a, b). Subsequent to the 1980 seepage study, a drainage blanket with a sub-drain system was installed to mitigate downstream seepage. Flow net analysis provided by Cedergren (1980a, b) suggests that the primary seepage mechanism involves flow through the dam foundation due to normal reservoir pool elevations, which results in upflow that intersects the ground surface in several areas on the downstream side of the dam. In addition to the reservoir pool elevations and downstream surface topography, flow is also controlled by the existing foundation geology as well as the presence or absence of a horizontal drain in the downstream portion of the dam.

The current modeling study is aimed at quantifying how variability in dam and foundation hydrologic properties influences seepage as a function of reservoir stage. Flow modeling is implemented using the COMSOL Multiphysics software package, which solves the partially saturated flow equations in a two-dimensional (2D) cross-section of Hidden Dam that also incorporates true downstream topography. Use of the COMSOL software package provides a more quantitative approach than the flow net analysis by Cedergren (1980a, b), and allows for rapid evaluation of the influence of various parameters such as reservoir level, dam structure and geometry, and hydrogeologic properties of the dam and foundation materials. Historical observation-well data are used to help validate the flow simulations by comparing observed and predicted water levels for a range of reservoir elevations. The flow models are guided by, and discussed in the context of, the geophysical work (Minsley and others, 2010) where appropriate.

Background

Location and Geology

Hidden Dam is located on the Fresno River in the Sierra Nevada foothills, approximately 15 miles northeast of Madera, California (figure 1). Detailed information regarding the dam construction and local geology and hydrology, summarized below, is provided by the U.S. Army Corps of Engineers (1977) as well as Cedergren (1980a, b). Hidden Dam is a rolled earthfill dam constructed between 1972 and 1975, with a crest length of approximately 5,700 ft, a maximum height above streambed of 184 ft, and a crest elevation of 561 ft. At gross pool (elevation of 540 ft), the impounded lake has a surface area of about 1,570 acres and a storage capacity of 90,000 acre-feet. Relief at the dam site is approximately 180 ft with elevations ranging between about 400 ft at the streambed to approximately 580 ft on the right and left abutments. This topography is characterized by gently rolling, rounded hills with scattered rock outcrops.

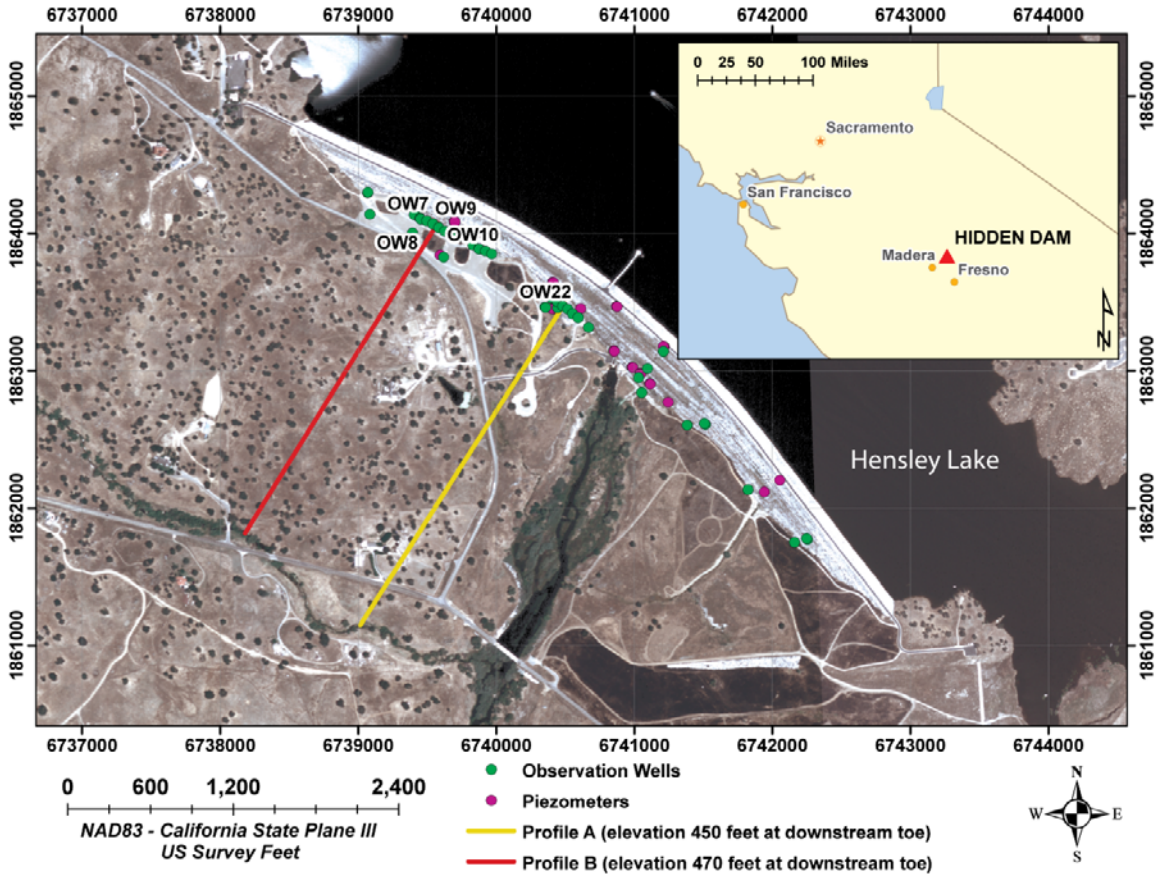

Figure 1. Location (inset) and aerial photo of Hidden Dam. Colored lines indicate topographic profiles that are used in the flow modeling study. Observation wells discussed in this report are labeled.

The area in the vicinity of Hidden Dam is underlain by what is generally described as granitic and associated metamorphic rocks derived from the Sierra Nevada batholith, though there is some variability in composition, texture, and color (U.S. Army Corps of Engineers, 1977). Granitic rocks are overlain by residual soil, slope wash, and alluvium, ranging in thickness from zero to approximately 30 ft and varying in composition between sands,

silts, and clays. Beneath the overburden, to total depths of up to 60 ft, the granite is decomposed such that it is easily crumbled or broken. Fresh rock occurs below the decomposed granite, though decomposed materials are occasionally interspersed up to depths of 140 ft. Jointing was observed throughout the foundation area during excavation, though the profusion of joints and the extent to which they are clay-filled varies throughout the site.

Summary of Previous Work

Studies carried out by Cedergren (1980a, b) highlighted the right, or northwest, side of the dam as the primary area of seepage concern. Part of these studies included several flow net calculations based on different characteristic sections of the dam that capture variability in downstream topography and horizontal drainage in the downstream portion of the dam. Initial estimates of hydraulic conductivity for the foundation and core materials resulted in seepage rates that did not match observed values, and revised hydraulic conductivity values were determined that provided a match between observed and predicted seepage (Cedergren, 1980a). A second set of flow net calculations were calibrated to new observation-well data, and predicted substantially higher water levels in several downstream locations for gross pool (540 ft) conditions. All of the flow net calculations were presented for gross pool conditions and did not incorporate any effect of the grout curtain located beneath the dam foundation.

More recently, geophysical surveys conducted in May 2009 at Hidden Dam focused on (1) assessing seepage through the use of self-potential measurements and (2) characterizing heterogeneity in the subsurface that might influence seepage patterns using direct current (DC) resistivity measurements (Minsley and others, 2010). The reservoir elevation at the time of the self-potential survey was approximately 490 ft, resulting in significantly less seepage than expected when the reservoir is at or near gross pool. The self-potential data highlighted several diffuse seepage areas on the right side of the dam that were consistent with the areas of previously known seepage. Additionally, one area of potentially focused seepage was identified above the outlet works. There was no evidence for significant amounts of seepage on the left side of the dam, which is also consistent with previous observations from the site (Cedergren, 1980a).

The DC resistivity data showed a resistive feature at approximately 0- to 80- ft depths along most of the right side of the dam, which was interpreted to be relatively unweathered and low-porosity granitic bedrock (figure 2). In general, this bedrock is expected to have relatively low hydraulic conductivity, but it is possible that there are localized seepage pathways in this unit due to the presence of joints. At the surface, lower resistivity values were interpreted as a combination of alluvial overburden and decomposed, or weathered, granitic bedrock that likely have higher hydraulic conductivity. One notable feature in the resistivity data is the presence of a wide (300–400 ft), intermediate-resistivity channel on the right side of the dam, which may be a significant pathway for increased flow underneath the dam. This feature is coincident with the broad self-potential anomaly in the low-topography area on the right side of the dam, which lends further evidence to the fact that this is an area of enhanced seepage.

Hidden Dam Flow Simulations

Description of Model

Two-dimensional (2D) numerical models of variably saturated flow at Hidden Dam were constructed using the COMSOL Multiphysics 3.5a finite element modeling software. The models simulate pressure head and flow distributions in the dam and surrounding foundation materials by solving the steady-state

Richards equation (Freeze and Cherry, 1979), where the van Genuchten (1980) parameterization is used to describe the saturation-dependent hydraulic properties (see Appendix). The models are used to assess the potential for seepage at the dam for several scenarios that include variability in the reservoir

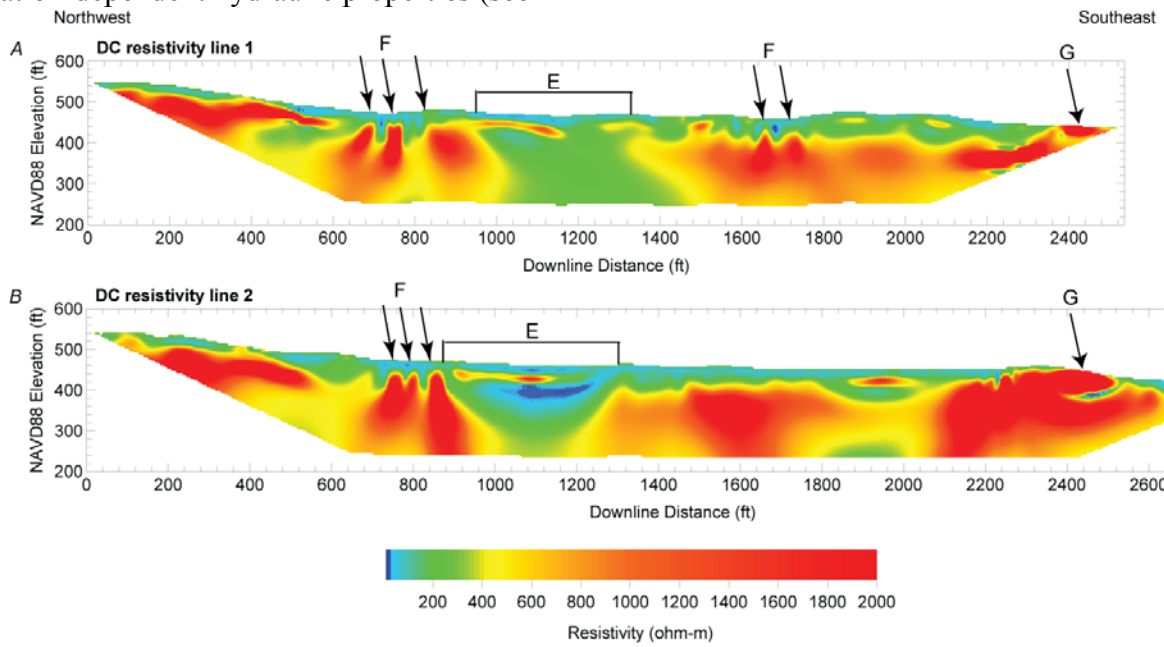

Figure 2. Inverted sections for DC resistivity (A) line 1 and (B) line 2 (from Minsley and others, 2010) at 1:1 scale. Location E, observed on both lines, is interpreted to be a deep alluvial valley between bedrock highs; locations F are highly resistive features that may represent competent granitic highs with complex geometry; and locations G illustrate high near-surface resistivity associated with large granite outcrops.

elevation, internal dam structure, and foundation structure. The DC resistivity survey results (Minsley and others, 2010) are used to help inform likely scenarios for subsurface hydraulic conductivity variability. Additionally, self-potential signals are predicted for the various flow models by incorporating electrokinetic coupling in COMSOL, as described in the Appendix.

The basic model geometry was constructed to match the dam design specifications (U.S. Army Corps of Engineers, 1977; Cedergren, 1980a) as closely as possible, and downstream topographic profiles were extracted from a 30-ft resolution digital elevation model (DEM) of the surrounding terrain. The model geometries shown in figure 3 and 4 correspond to profiles A and B shown in figure 1, where the elevation at the downstream toe is approximately 450 and 470 ft, respectively. Each model includes subdomains representing bedrock (BR), the central impervious core (IC), the outer shell comprising random fill materials (RF), transition and outer shell zones comprising select fill materials (SF), the vertical chimney drain comprising drainage fill materials (DF), and the impervious grout curtain (GC) beneath the dam foundation.

The model geometries in figure 3 and 4 and the hydrologic parameters for each unit summarized in table 1 are used as the ‘baseline’ models for this study. Saturated hydraulic conductivity values were taken from Cedergren (1980a), with the exception of the grout curtain, which was not incorporated in previous studies. The saturated and residual moisture content, as well as parameters a (related to the air entry pressure head and desorption behavior of the soil) and n (related to the pore-size distribution of the soil), were derived according to the

procedure discussed in the Appendix from information in the foundation report (U.S. Army Corps of Engineers, 1977) and Cedergren (1980a) for all units except for the bedrock and grout curtain, which did not have the necessary input data. Default values have been used for the hydrologic parameters where no information was available. Results from these baseline models, as well as several variations on the geometry and hydrologic properties, are discussed in the following sections. For convenience, the figures from all of the scenarios have been placed together at the end of this report..

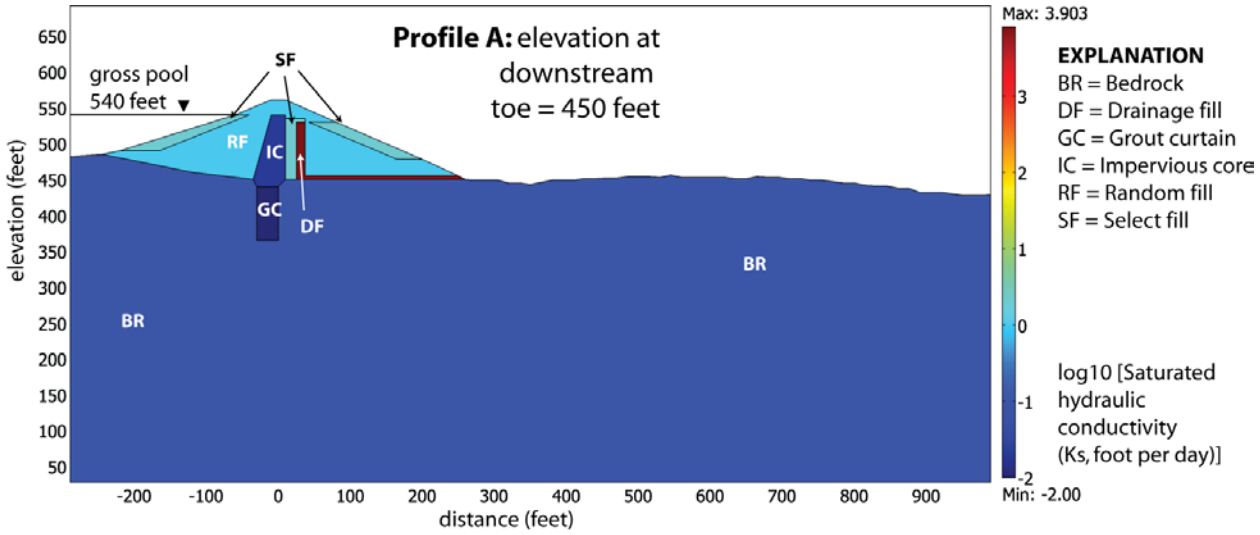

Figure 3. Geometry of Hidden Dam and downstream topography along profile A in figure 1. Color scale indicates the baseline saturated hydraulic conductivity values used in this study.

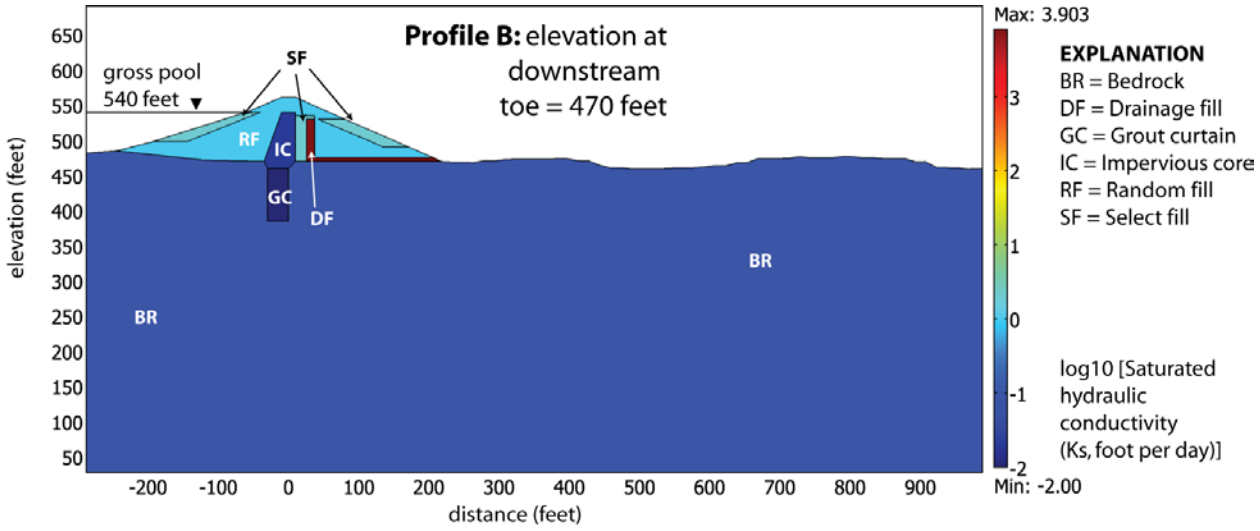

Figure 4. Geometry of Hidden Dam and downstream topography along profile B in figure 1. Color scale indicates the baseline saturated hydraulic conductivity values used in this study.

Table 1. Baseline parameters for each Hidden Dam unit used in the variably saturated flow model.

	Saturated hydraulic conductivity, K_s (ft/day)	Saturated moisture content, θ_s (volume fraction)	Residual moisture content, θ_r (volume fraction)	a (1/ft)	n	Water density, ρ (lb/ft^3)	Fluid source, Q_s (1/s)
Bedrock (BR)	0.1	0.150	0.050	0.2000	2.000	62.42	0
Impervious core (IC)	0.02	0.418	0.210	0.2013	1.9923		
Random fill (RF)	1.0	0.372	0.015	0.2399	3.9218		
Select fill (SF)	2.0	0.375	0.014	0.2453	3.3088		
Drainage fill (DF)	8,000.0	0.425	0.020	0.7165	3.5952		
Grout curtain (GC)	0.01	0.05	0.005	0.2000	2.0000		

Scenario 1: Baseline Model, Profile A

This first scenario illustrates the difference in flow for the baseline model along profile A at reservoir elevations between 480 and 540 ft. The baseline models have identical material properties for the various dam and bedrock units (table 1), but differ in downstream topography profiles. The elevation at the downstream toe on profile A is 450 ft, and there is a low-topography area approximately 100 ft from the toe of the dam, or at about 350 ft downline distance on the model. This geometry and parameters for this scenario are similar to flow net number 2 produced by Cedergren (1980a).

Figure 5–7 show the flow model results for profile A with reservoir elevations 485, 510, and 540 ft. Increasing saturation and flow through the dam are evident as the reservoir elevation increases. In each of these figures, the length of the white arrows represent relative variations in flow velocity in a model, but do not indicate absolute differences in flow velocity between models. The effectiveness of the high-hydraulic-conductivity horizontal-drainage fill on the downstream side of the dam is evident in these figures, as the drainage fill prevents increased water levels and redirects upward flow in the foundation materials out toward the toe. Saturation in the high-topography areas downstream of the dam can also be seen to increase as the reservoir elevation increases. Focused seepage is also evident in the low-topography area at approximately 350 ft downline distance , and becomes more enhanced at higher reservoir elevations. This observation of focused seepage in the low-topography area is consistent with observations of seepage at Hidden Dam (Cedergren, 1980a).

Seepage through the downstream embankment and ground surface is quantified in figure 8, which shows the rate of seepage (ft/s) along the surface model boundary as a function of distance for the models shown in figure 5–7. The sharp spike at a distance of approximately 260 ft corresponds to the outward flow through the conductive drainage-fill material at the toe of the dam. Discrete zones of seepage are evident in the low-topography areas from 300–400 ft, as well as 900–1,000 ft. This latter seepage zone is another low-topography area, which can be seen in figure 3. As expected, the rate of seepage increases with reservoir elevation. In some cases (just past 400 ft, for example), seepage only begins at the higher reservoir elevations.

Further quantification of seepage for this model is shown in figure 9, which shows volumetric flow (gal/min) through the

downstream embankment (blue) and ground surface (red) per foot along the length of the dam as a function of reservoir elevation. The volumetric flow is calculated by integrating the seepage along both the downstream embankment and ground surface boundaries in the model. An increasing proportion of flow through the dam can be seen with increasing reservoir elevation, to a maximum of approximately 0.055 gal/min per ft of total seepage at gross pool. This is consistent with, but slightly greater than, the approximately 0.04 gal/min per ft for flow net number 2 produced by Cedergren (1980a).

Figure 10 illustrates simulated observation-well data that can be obtained from the flow model results. Each panel shows the predicted water level in an observation well relative to the ground surface, where positive values are higher than the ground surface, for different reservoir elevations and any well depth between zero and 50 feet. That is, for a given observation well depth and reservoir elevation, the predicted water level in the well can be found on one of the curves in the figure. The panel on the left is for an observation-well approximately 15 ft from the downstream toe, which is a typical location for a number of observation wells at Hidden Dam. The panel on the right is for an observation well approximately 90 ft from the downstream toe, which corresponds to a low-topography area of focused seepage.

The model-predicted water levels are consistent with observation-well data reported in the 1980 seepage study (Cedergren, 1980b). Although the observed and model-predicted water levels are consistent, some discrepancy can be expected due to (1) the fact that the ground surface elevations for the flow model do not exactly match the observation wells, (2) hydrogeologic heterogeneity is not captured in the flow model, and (3) the three-dimensional nature of flow is not captured in the two-dimensional flow model.

For example, water levels in observation wells OW-9 and OW-10, which are located in areas of relatively low topography away from the downstream toe (figure 1), were 2–5 ft above ground surface at the reservoir elevation of approximately 484 ft (see table 1 in Cedergren, 1980b). Given the well depth of approximately 22 ft for these wells, the model-predicted water level on the right panel in figure 10 is around 4 ft above the ground surface for the curve that corresponds to a reservoir elevation of 485 ft. Observed water levels in wells OW-7A/B and OW-8A/B, which are close to the downstream toe, were approximately 2 ft and –2ft with respect to the ground surface, respectively. The model-predicted water level for wells close to the downstream toe at a reservoir elevation of 485 ft is less than 1 ft below ground surface (figure 10, left panel), which is consistent with the observed values. A key benefit of the flow modeling is that water levels can be predicted for any reservoir elevation or observation-well depth. As can be seen in figure 10, the maximum expected water level for this model geometry is approximately 8 ft above the ground surface for a 50-ft-deep well located 90 ft from the downstream toe.

Figure 11 shows the self-potential values predicted along the ground surface and downstream embankment for the flow depicted in figure 5–7 (reservoir elevations 485, 510, and 540 ft). The self-potential values are calculated by incorporating electrokinetic coupling into the COMSOL model, as described in the Appendix. The self-potential values depend on the flow velocity, electrical resistivity structure, and excess charge in the pore space. The latter two values are automatically calculated using empirical relationships that are also discussed in the Appendix. The self-potential values displayed in figure 11 are relative to an arbitrary reference location, which was chosen at the crest of the dam (distance equals 0 ft).

There are four main components to the self-potential signal that can be attributed to details in the flow model:

1. General trend of increasing potentials with distance: This trend represents the expected

response of increasing self-potentials in the direction of flow (Morgan and others, 1989; Minsley and others, 2010).

2. Trend of increasing potentials with increasing reservoir level: Because the self-potentials are proportional to flow, as described in equation (6) in the Appendix, increased flow due to higher reservoir elevations leads to increased self-potentials
3. Positive "kicks" superimposed on the general trend: Seepage outflow areas are expected to result in positive self-potential anomalies. This is related to item (1) above, as the seepage areas represent localized flow terminations and, correspondingly, maximum self-potentials at those locations.
4. Sharp trend in self-potentials between 0–100 ft, increasing with reservoir elevation, and a negative center at the highest reservoir elevation: This trend near the dam crest is due to the increasing downward component of flow as seepage passing through the impervious core is rapidly transported through the drainage fill. In contrast with the seepage outflow areas that generate a positive anomaly, this downward flow-zone generates a negative anomaly. Because the flow magnitude increases with increasing reservoir elevation, the strength of the negative self-potential anomaly increases proportionally.

The self-potential data collected at Hidden Dam (Minsley and others, 2010) clearly indicate localized positive anomalies on the order of 30–70 mV in the low-topography seepage areas, which is consistent with the coupled flow modeling result. The data do not clearly indicate an overall trend of increasing potentials in the downstream direction, though this is difficult to identify due to the location of survey lines, which were primarily in the dam-parallel direction. Additionally, there is clearly a three-dimensional component to the flow and corresponding self-potentials due to variations in the ground-surface topography both along and perpendicular to the dam strike.

An example of the electrical resistivity structure determined from the flow model at a reservoir elevation of 510 ft is shown in figure 12. The resistivity values are calculated using equation (7) in the Appendix, where a constant water resistivity of 20 ohm-m and cementation factor, m, of 1.7 are assumed. The bedrock resistivity of 500 ohm-m is similar to the values observed during the geophysical surveys at Hidden Dam (Minsley and others, 2010), though the field data suggest a primarily two-layer model with lower near-surface resistivity, which is investigated in modeling scenarios 4 and 5. Very high resistivities (greater than 10,000 ohm-m) are observed in the unsaturated portions of the dam. The resistivity information is an important part of calculating self-potential values, but could also be used to guide future geophysical investigations at the site.

Scenario 2: Baseline Model, Profile B

This flow scenario follows the same modeling procedures as with the previous example, but uses the model geometry for profile B (figure 4) along with the baseline model parameters (table 1). Profile B is located closer to the right abutment than profile A (figure 1), and therefore has higher ground surface elevations (470 ft at the downstream toe) than profile A. A second difference with this profile is the details of the downstream topography. Along profile B, the ground surface dips only slightly near the downstream toe, then rises again over one of the rounded hills found in the right abutment area before dropping approximately 20 ft to a low-topography area that coincides with the area covered by the drainage blanket. As with scenario 1, the low-topography areas are significant factors in the distribution of seepage.

Figure 13–15 show results from the flow model at 485-, 510-, and 540-ft-reservoir elevations. As with scenario 1, the effectiveness of the horizontal drainage fill is evident as it redirects upward seepage beneath

the dam toward the downstream toe rather than into the dam structure. The main difference with this flow scenario is the distribution of seepage in low-topography areas; particularly between 450–650 ft, but also somewhat near the downstream toe. Additionally, the uppermost part of the hill between 250–450 ft remains unsaturated at the lower reservoir elevations, but becomes almost entirely saturated at gross pool.

Seepage through the downstream embankment and ground surface is quantified in figure 16, which shows the rate of seepage (ft/s) along the surface model boundary as a function of distance for the models shown in figure 13–15. The sharp spike at a distance of approximately 220 ft corresponds to the outward flow through the conductive drainage-fill material at the toe of the dam. Discrete zones of seepage are evident on either side of the hill area from 220–280 ft and 450–600 ft, as well as another low-topography area farther downstream at 900–1,000 ft. As expected, the rate of seepage increases with reservoir elevation.

Figure 17 shows the volumetric flow (gal/min) through the downstream embankment (blue) and ground surface (red) per foot along the length of the dam as a function of reservoir elevation. As with scenario 1, an increasing proportion of flow through the dam can be seen with increasing reservoir elevation, to a maximum of approximately 0.0425 gal/min per ft at gross pool. This is also very consistent flow net number 2 produced by Cedergren (1980a), which predicted approximately 0.04 gal/min per ft. The reduced seepage compared with scenario 1 is due to the higher downstream elevation in this case. For the lowest reservoir elevation (480 ft), virtually all of the seepage is through the downstream ground surface.

Figure 18 illustrates simulated observation-well data that can be obtained from the flow model results. Each panel shows the predicted water level in an observation well relative to the ground surface, where positive values are higher than the ground surface (that is, artesian conditions), for different reservoir elevations and any well depth between 0 and 50 ft. That is, for a given observation-well depth and reservoir elevation, the predicted water level in the well can be found on one of the curves in the figure. The panel on the left is for an observation well approximately 15 ft from the downstream toe, which is a typical location for a number of observation wells at Hidden Dam. The panel on the right is for an observation well approximately 300 ft from the downstream toe, which corresponds to a low-topography area of focused seepage.

The simulated observation-well results are similar to those for scenario 1, with a few minor differences. For example, the water level predicted for any well depth at the location 15 ft downstream from the toe is approximately 2 ft below ground surface for the 480-ft reservoir elevation in scenario 2, whereas it is much closer to the ground surface in scenario 1. Additionally, at a reservoir elevation of 485 ft, the predicted water level on the left panel of figure 18 is above the ground surface, whereas the corresponding curve in figure 10 indicates a water level slightly below ground surface. This is somewhat counterintuitive as one might expect the lower topography scenario (scenario 1) to have the higher predicted water levels, and highlights the nonlinearity in predicted water level as a function of model geometry.

Figure 19 shows the self-potential values predicted along the ground surface and downstream embankment for the flow depicted in figure 13–15 (reservoir elevations 485, 510, and 540 ft). The self-potential values displayed in figure 19 are relative to an arbitrary reference location, which was chosen at the crest of the dam (distance equals 0 ft).

Scenario 3: Profile A, No Horizontal Drainage Fill

This flow scenario is identical to scenario 1, with the exception that there is no horizontal drainage-fill material along the downstream base of the dam, and is similar to flow net 1 produced by Cedergren (Cedergren, 1980a). Absence of the high-hydraulic-conductivity horizontal-drainage fill results in elevated water levels in the downstream portion of the dam, which can be seen in the flow model results in figure 20–22. This increased flow through the dam, as well as elevated hydraulic pressure relative to the baseline models, could be a mechanism for internal erosion over long periods of time.

Although there is clearly a larger region of seepage in the dam and downstream embankment, the seepage pattern along the downstream topography is not significantly different. This is quantified in figure 23, which shows the rate of seepage (ft/s) along the model boundary as a function of distance for the models shown in figure 20–22. In this scenario, the increased seepage face along the downstream embankment is evident as a broader zone of flow between 240–260 ft in figure 23, compared with the very sharp outflow spike at the downstream toe in figure 8. Discrete zones of seepage are evident in the low-topography areas from 300–400 ft, as well as 900–1,000 ft, and are similar in magnitude to scenario 1. One interesting feature is the increased seepage areas between 400–500 ft compared with scenario 1. This is likely due to the fact that the net hydraulic conductivity of the dam is reduced with the removal of the drainage-fill material, which partitions a greater amount of seepage into the foundation below the dam that exits further downstream.

Figure 24 shows the volumetric flow (gal/min) through the downstream embankment (blue) and ground surface (red) per foot along the length of the dam as a function of reservoir elevation. As with scenario 1, an increasing proportion of flow through the dam can be seen with increasing reservoir elevation, to a maximum of approximately 0.0425 gal/min per ft at gross pool. It is interesting that the total seepage in scenario 3 is less than scenario 1 at all reservoir elevations (0.055 gal/min at gross pool for scenario 1 versus 0.0425 gal/min at gross pool for scenario 3). Additionally, a much greater proportion of seepage in scenario 3 flows through the ground surface instead of the downstream embankment compared with scenario 1. This can be explained by the fact that, while the seepage face along the downstream embankment is wider in scenario 3, the high-hydraulic conductivity drainage-fill material in scenario 1 drains significantly more water through the dam.

The predicted observation-well water levels in figure 25 are elevated with respect to the predicted water levels for scenario 1 (figure 10), and this difference becomes more pronounced as the well depth and/or reservoir elevation increases. Significant pressures at depth corresponding to water levels of 10–12 ft above the ground surface are predicted for the highest reservoir elevations. This observation is consistent with the argument that the reduced net-hydraulic conductivity of the dam due to the lack of horizontal-drainage fill causes more seepage to be partitioned into the subsurface beneath the dam, contributing to increased pressure at depth. It is possible that an analysis of observation-well data could be used to assess the effectiveness of the horizontal drain along the length of the dam, though it is important to note that other factors such as local hydrogeologic heterogeneity can influence these observations.

Figure 26 shows the self-potential values predicted along the ground surface and downstream embankment for the flow depicted in figure 20–22 (reservoir elevations 485, 510, and 540 ft). The self-potential values displayed in figure 26 are relative to an arbitrary reference

location, which was chosen at the crest of the dam (distance equals 0 ft).

The self-potentials for scenario 3 are very similar to scenario 1 (figure 11), with a few exceptions. First, the magnitude of the seepage-related self-potential anomalies between 250–450 ft are more pronounced in scenario 3, again reflecting the increased amount of subsurface flow relative to scenario 1. Second, the shape of the self-potential curves from 0–250 ft are different for the two scenarios, reflecting the difference in internal flow patterns in the dam structure and shallow foundation. Measurements in this area could be very diagnostic about flow in the dam structure, though good measurements are difficult to make over the dam structure due to the difficulty in obtaining good electrical contact over riprap-covered surfaces (Minsley and others, 2010).

Scenario 4: Profile A, Baseline Model with Near-Surface Sediment Layer

Flow scenario 4 uses the profile A baseline model as in scenario 1, but with the addition of a variable-thickness layer in the near-surface on the downstream portion of the model that has a higher saturated hydraulic conductivity than the bedrock (figure 27). Justification for the addition of this layer comes from the known presence of residual soil, slope wash, alluvial sediments, and decomposed granite that overlie bedrock (U.S. Army Corps of Engineers, 1977; Cedergren, 1980a), as well as the two-layer resistivity model observed over the downstream portion of the dam foundation (Minsley and others, 2010) that is consistent with higher hydraulic conductivity sedimentary overburden. Hydraulic parameters used for this sediment layer are: K_s = 0.5 ft/day, θ_s = 0.25, θ_r = 0.015, a = 0.2399 1/ft, n = 3.9218.

The flow modeling results in figure 28–30 are similar to those in scenario 1 (figure 5–7) with a few minor exceptions. Although the drainage-fill material still serves as an effective cutoff for upward flow coming from the foundation, an increased amount of downstream-oriented seepage is focused in the sediment layer due to its elevated hydraulic conductivity with respect to the bedrock. Additionally, the elevated hydraulic conductivity and saturated moisture content of the sediment layer limits the saturation in some of the high-topography hill areas downstream of the dam, even at gross pool.

The rate of seepage (ft/s) along the model boundary as a function of distance for the models shown in figure 28–30 is illustrated in figure 31. Compared with the corresponding image for scenario 1 (figure 8), it is clear that the impact of the high-hydraulic-conductivity sediment layer has not significantly altered the distribution of seepage, but the seepage rate has increased by a factor of 2–3.

Figure 32 shows the volumetric flow (gal/min) through the downstream embankment (blue) and ground surface (red) per foot along the length of the dam as a function of reservoir elevation. The maximum of approximately 0.057 gal/min at gross pool is close to the scenario 1 value of 0.055 gal/min (figure 9), and the total rate of seepage at other reservoir elevations are also comparable between the two models. In scenario 4, however, it is apparent that a greater amount of the volumetric seepage occurs through the downstream ground surface rather than the embankment when compared with scenario 1. This is again consistent with the observation that the elevated hydraulic conductivity of the sediment layer directs an increased amount of flow in the downstream direction away from the dam.

The predicted observation-well water levels for scenario 4 are illustrated in figure 33. The water levels are significantly reduced with respect to scenario 1 (figure 10), with a maximum predicted water level of approximately 4 ft above ground surface at gross pool for a 50-ft-deep well. The ‘kink’ in the curves at approximately 40-ft depth corresponds to the transition from the sediment

layer to bedrock. The reduced water levels predicted for scenario 4 are a direct result of the elevated hydraulic conductivity, which acts to reduce hydraulic pressure in the subsurface.

Figure 34 shows the self-potential values predicted along the ground surface and downstream embankment for the flow depicted in figure 28–30 (reservoir elevations 485, 510, and 540 ft). The self-potential values are relative to an arbitrary reference location, which was chosen at the crest of the dam (distance equals 0 ft). The self-potential response for scenario 4 is very similar to scenario 1 (figure 11), both in character and magnitude, though the self-potential values in flow scenario 4 are slightly smaller. This is somewhat non-intuitive due to the increased seepage rate with respect to scenario 1 (figure 31), but results from the fact that the elevated hydraulic conductivity sediment layer leads to reduced excess charge in equation (8) and the elevated saturated moisture content of the sediment layer leads to reduced electrical resistivity according to equation (7), both of which lead to reduced self-potential values as described in the Appendix.

The electrical resistivity profile for this flow model derived using equation (7) and a reservoir elevation of 510 ft is shown in figure 35. The resistivity of the near-surface sediment layer is approximately 200 ohm-m, which is consistent with the values reported from the geophysical field survey (Minsley and others, 2010). One important factor that is not accurately accounted for in this flow model is the thickness profile of this sediment layer. Because the resistivity surveys were oriented parallel to the dam, this information could not be incorporated into the flow models beyond the use of a 'typical' thickness observed from the resistivity profiles.

Scenario 5: Profile A, Baseline Model with Deep Sediment Channel

Flow scenario 5 uses the profile A baseline model as in scenario 1, but with the addition of a thick (several hundred feet) sediment channel that extends from the upstream to downstream portions of the model (figure 36). Justification for the addition of this deep channel comes from the resistivity survey at Hidden Dam (Minsley and others, 2010) that identified a wide (300–400 ft), low-resistivity channel that extends to depths of several hundred feet over a portion of the low-topography area downstream of the dam (figure 2). Hydraulic parameters used for this sediment channel are the same as those used in scenario 4: K_s = 0.5 ft/day, θ_s = 0.25, θ_r = 0.015, a = 0.2399 1/ft, n = 3.9218.

The flow modeling results in figure 37–39 are more similar to those in scenario 1 (figure 5–7) than to the sediment layer case in scenario 4 (figure 28–30). In scenario 5 the hydraulic conductivity in the foundation is controlled mainly by the sediment channel (K_s = 0.5 ft/day), compared with scenario 1, where the foundation is bedrock (K_s = 0.1 ft/day). One similarity with scenario 4, however, is the reduced saturation in the high-topography hill area downstream of the dam due to the elevated hydraulic conductivity.

The rate of seepage (ft/s) along the model boundary as a function of distance for the models shown in figure 37–39 is illustrated in figure 40. The seepage pattern is similar to scenario 1 (figure 8), but the magnitude of the rate of seepage is similar to (but somewhat larger than) scenario 4 (figure 31). The high-hydraulic-conductivity sediment channel that extends to the upstream side of the dam results in seepage rates that are approximately 3–4 times greater than the baseline case in scenario 1.

Figure 41 shows the volumetric flow (gal/min) through the downstream embankment (blue) and ground surface (red) per foot along

the length of the dam as a function of reservoir elevation. The maximum of approximately 0.162 gal/min at gross pool is significantly larger than the scenario 1 or scenario 5 values of approximately 0.055 gal/min (figure 9 and 32). This increased volumetric rate of seepage is consistent with the value of 0.108 gal/min reported by Cedergren (1980a, table 6) for a slightly lower foundation hydraulic conductivity of 0.25 ft/day.

The predicted observation-well water levels for scenario 5 are illustrated in figure 42. The water levels are very similar to those predicted in scenario 1 (figure 10), with a maximum predicted water level of approximately 7 ft above ground surface at gross pool for a 50-ft-deep well. Although the seepage rate is much higher than in scenario 1, the effect of the elevated hydraulic conductivity reduces pressures at depth and results in similar predicted water levels.

Figure 43 shows the self-potential values predicted along the ground surface and downstream embankment for the flow depicted in figure 37–39 (reservoir elevations 485, 510, and 540 ft). The self-potential values are relative to an arbitrary reference location, which was chosen at the crest of the dam (distance equals 0 ft). The self-potential response for scenario 5 is very similar to scenario 1 (figure 11) and scenario 4 (figure 34), both in character and magnitude, though the self-potential values in flow scenario 5 are slightly smaller. This is due to the same effect discussed in scenario 4, where the reduced excess charge in equation (8) and the reduced electrical resistivity according to equation (7) counteract the increased seepage rate and leads to reduced self-potential magnitudes as described in the Appendix.

Comparison with Selected Observation-Well Data

Historical reservoir elevation data, along with measurements from observation wells, piezometers, and weirs, were obtained for the Hidden Dam site (K. Hazleton, written commun., 2009). These records provide useful information regarding the connection between reservoir elevation and downstream water levels and seepage at the site. Here, we focus on the records for two observation wells on the right abutment drainage blanket area with elevations that are comparable to the surface elevations on the two profiles used in this study (figure 1). OW-22 has an elevation of approximately 450 feet, with a screened depth between 15–20 feet. OW-7 has an elevation of approximately 470 feet, with a screened depth interval between 30–40 feet. Figure 44 shows the historical record of reservoir elevation (top panel) as well as water levels relative to the ground surface (negative values are below ground) for these wells (lower panels) since 1980.

A more detailed view of these curves is provided in figure 45, which overlays the reservoir elevation and observation-well records for the years 2001–2004. Water levels in the observation wells are a damped version of the forcing produced by variations in the reservoir elevation, with a clear time-shift between the two curves that indicates a characteristic reaction time for seepage through the dam.

In figure 46, the reservoir elevation data are cross-plotted with the observation-well water levels for OW-22 (A) and OW-7 (B) for the entire available historical record. As expected, there is a positive correlation between reservoir elevation and observed water level, with a slope of approximately 0.1 and 0.2 in OW-22 and OW-7, respectively (that is, a 1-ft increase in reservoir elevation leads to approximately 0.2-ft increase in observation-well levels in OW-7). The large number of zero-values and absence of

positive water levels in the OW-22 data indicate the inability to record water levels that are higher than the ground surface. Values extrapolated to gross pool using the slope of 0.2 are approximately 8 ft above ground. In OW-7, above-ground water levels are measured with pressure transducers.

Superimposed on the observation-well data are the model-predicted water levels from the various flow scenarios in this study taken from the appropriate well depths in figure 10 (scenario 1), figure 18 (scenario 2), figure 25 (scenario 3), figure 33 (scenario 4), and figure 42 (scenario 5). There is a reasonably good agreement between the observation-well data and model-predicted water levels, suggesting that the flow models in this study provide a good representation of seepage at Hidden Dam, though the flow models tend to predict water levels that are slightly elevated for specific reservoir elevations. This discrepancy may be related to inaccuracies in the details of the model geometry or hydrologic properties, as well as the fact that there is a 3D component of flow that is not captured in the 2D models. One notable feature in the simulated water-level data is the nonlinear aspect that is apparent as a decrease in slope at higher reservoir elevations, which is also apparent in the historical record data in figure 46B.

In figure 46A, it is evident that the predictions for the scenario 4 model, which involves the thin sediment (higher hydraulic conductivity) layer over bedrock (figure 27), correspond most closely with the historical record. The lack of historical data for positive water levels, however, makes it impossible to validate this observation for reservoir elevations above 510 ft. Agreement with the historical data, along with the fact that scenario 4 is consistent with the hydrogeologic knowledge of the site as well as the general character observed in the DC resistivity models (figure 2) over much of the right abutment area, suggests that this is a reasonable model for flow through the portion of the dam in the vicinity of OW-22.

Conclusions

Quantitative information about seepage and flow patterns at Hidden Dam is provided by this numerical modeling study. The flow model scenarios, dam geometry, and hydrologic parameters were guided by the foundation report and initial flow net studies (U.S. Army Corps of Engineers, 1977; Cedergren, 1980a), with additional information about subsurface structural properties inferred from more recent geophysical work (Minsley and others, 2010). Implementation of the variably saturated flow equations in COMSOL allows for quantitative predictions of seepage rates or volumes, water levels, and degree of saturation anywhere in the model as a function of changing reservoir elevation. This provides a valuable framework for studying different hydrogeologic or dam-structure scenarios. The modeling results are consistent with both the initial flow net studies (Cedergren, 1980a) as well as data from observation wells at the site.

Additionally, we have provided a methodology for coupling the flow results to geophysical properties investigated by Minsley and others (2010). The predicted electrical resistivity model for any flow scenario is determined through a petrophysical relationship that incorporates the calculated total moisture content. This electrical resistivity model is subsequently used in a second set of equations that describe the self-potential response to the various flow scenarios based on electrokinetic coupling. Predicting the geophysical response to various hydrogeologic models helps to validate the field data already acquired, but also provides useful information for guiding future geophysical studies. The expected geophysical response to different flow scenarios can be used to guide survey locations and acquisition parameters that will be most sensitive to subsurface changes of interest.

Several of the main insights gained from this study are outlined below:

- Low-topography areas act to focus seepage, which is consistent with historical observations at the site. Low-topography areas can also result in seepage at significant distances downstream of the dam (for example, 900–1,000 ft in figure 8). Cedergren (1980a) identified one such area approximately 700 ft downstream on the left side of the dam.

- Predicted water levels are near or above the ground surface for reservoir elevations above 480 ft in all of the scenarios studied. The maximum value in this study is approximately 12 ft above ground surface for scenario 3 (no horizontal drainage fill, figure 25). Water levels do not, however, reach the extremely high values up to 40 feet above the ground surface at gross pool predicted in the revised flow net study by Cedergren (1980b)

- Absence of the horizontal drainage-fill material in the downstream part of the dam (scenario 3) results in a broader area of seepage on the downstream embankment (figure 20–22), but reduced volumetric seepage compared with the case where the drainage fill is present. This is because the absence of the drainage fill reduces the net hydraulic conductivity of the dam, which partitions a greater amount of seepage into the subsurface (compare figure 24 with figure 9). None the less, this enhanced area of flow in the dam may lead to increased long-term erosion under elevated reservoir levels.

- The presence of a thin (tens of feet) sedimentary layer with higher hydraulic conductivity than the underlying bedrock results in moderately increased seepage in the downstream area (compare figure 23 with figure 8) as well as a greater proportion of seepage in the sediment and bedrock (compare figure 24 with figure 9), but also results in lower water levels in observation wells (compare figure 25 with figure 10).

- The presence of a deep (hundreds of feet) sedimentary channel under the dam foundation, suggested by the resistivity survey carried out by Minsley and others (2010), leads to substantial increases in volumetric seepage under the dam (compare figure 41 with figure 9), though water levels predicted in observation wells are comparable to the case without a high-conductivity channel (compare figure 42 with figure 10). This observation of increased seepage, but unchanged water level (pressure), is predicted from normal Darcy flow (Freeze and Cherry, 1979): the increased hydraulic conductivity in the sediment channel leads to increased flow, but the pressure gradient (defined by the ratio of flow to hydraulic conductivity) remains unchanged. This suggests that water-level data alone may not be a good indicator of relative amounts of seepage along the dam if the wells are located in different geologic structures.

- For a given scenario, the predicted self-potential response scales with seepage due to increased flow. However, increased seepage at one location with elevated hydraulic conductivity does not necessarily lead to larger self-potentials than an area with lower hydraulic conductivity and reduced seepage (compare figure 43 with figure 11) due to the counteracting role of electrical resistivity and excess charge in the self-potential response. It is clear, however, that for the same bedrock hydraulic conductivity, increased self-potentials are observed when the horizontal-drainage fill is absent because of increased seepage beneath the dam (compare figure 26 with figure 11).

- The self-potential response over the downstream embankment for the case with

no horizontal drainage fill (figure 26) is different than when the drainage fill is present (figure 11) and becomes more apparent at higher reservoir elevations. While this could be a useful indicator of locations with effective drainage fill, self-potential measurements on riprap are difficult and would likely require dedicated holes into dam material to make good electrical contact.

- One limiting factor in this study is that 2D models are used, which assumes that all flow is perpendicular to the dam. While this is a reasonable modeling assumption, the true downstream topography likely produces a component of flow that is directed toward the outflow axis of the dam. Additionally, variability in internal dam structure (for example, the presence or absence of drainage fill) and subsurface heterogeneity (such as the influence of a deep sediment channel) may also lead to 3D flow patterns not captured in this study.

Acknowledgments

This work was carried out with the support of the U.S. Army Corps of Engineers, Sacramento District, under the supervision of Lewis Hunter. We thank Lewis Hunter, Kevin Hazleton, Beth Burton, and Martin Fahning for their reviews of the manuscript.

References Cited

Archie, G.E., 1942, The electrical resistivity log as an aid in determining some reservoir characteristics: Trans. Amer. Inst. Mining Metallurgical and Petroleum Engineers, v. 146, p. 54–62.

Cedergren, H.R., 1980a, Seepage study of Hidden Dam, Fresno River, California: Prepared for Department of the Army, Sacramento District, Corps of Engineers, 210 p.

Cedergren, H.R., 1980b, Seepage study of Hidden Dam, Fresno River, California: Analysis of data from observation wells put in right abutment seepage areas in 1980: Prepared for Department of the Army, Sacramento District, Corps of Engineers, 31 p.

Freeze, R.A., and Cherry, J.A., 1979, Groundwater: Englewood Cliffs, New Jersey, Prentice Hall, 604 p.

Ishido, T., and Mizutani, H., 1981, Experimental and theoretical basis of electrokinetic phenomena in rock-water systems and its applications to geophysics: Journal of Geophysical Research, v. 86, no. NB3, p. 1763–1775.

Jardani, A., Revil, A., Boleve, A., and Dupont, J.P., 2008, Three-dimensional inversion of self-potential data used to constrain the pattern of groundwater flow in geothermal fields: Journal of Geophysical Research-Solid Earth, v. 113, B09204.

Lesmes, D.P., and Friedman, S.P., 2005, Relationships between the electrical and hydrogeological properties of rocks and soils, *in* Rubin, Y., and Hubbard, S.S., eds., Hydrogeophysics: Netherlands, Springer, p. 87–128.

Minsley, B.J., Burton, B.L., Ikard, S., and Powers, M.H., 2010, Geophysical investigations at Hidden Dam, Raymond, CA: Summary of fieldwork and preliminary data analysis U.S. Geological Survey Open-File Report 2010-1013, 25 p.

Morgan, F.D., Williams, E.R., and Madden, T.R., 1989, Streaming potential properties of Westerly Granite with applications: Journal of Geophysical Research-Solid Earth and Planets, v. 94, no. B9, p. 12449–12461.

Revil, A., Pezard, P.A., and Glover, P.W.J., 1999, Streaming potential in porous media 1. Theory of the zeta potential: Journal of Geophysical Research-Solid Earth, v. 104, no. B9, p. 20021–20031.

Saxton, K.E., and Rawls, W.J., 2006, Soil water characteristic estimates by texture and organic matter for hydrologic solutions: Soil Science Society of America Journal, v. 70, no. 5, p. 1569–1578.

U.S. Army Corps of Engineers, 1977, Foundation report: Hidden Dam project, Hensley Lake, Fresno River, California, Madera County: USACE, Sacramento District.

van Genuchten, M.T., 1980, A Closed-form Equation for Predicting the Hydraulic Conductivity of Unsaturated Soils: Soil Science Society of America Journal, v. 44.

Appendix

Governing Variably Saturated Flow Equations

The formulation of the steady-state Richards equation solved by COMSOL Multiphysics is

$$\nabla \cdot \left(-\frac{K_s k_r}{\rho g}\left(\nabla p + \rho g \nabla z\right) \right) = Q_s \qquad (1)$$

where K_s is the saturated hydraulic conductivity (ft/s); ρ is the water density, which is set to a constant 62.42 lb/ft^3; g is the acceleration due to gravity, equal to 32.2 ft/s^2; p is the state variable that describes water pressure (lbf/ft^2) throughout the model; z is elevation (ft), and Q_s represents imposed fluid sources or sinks (1/s). The van Genuchten equations (van Genuchten, 1980) are used to describe the relative permeability, k_r, effective saturation, Se, and liquid volume, θ, as a function of pressure head, which is defined as $H_p = p/\rho g$ (ft).

$$k_r = \begin{cases} Se\left(1-\left(1-Se^{1/m}\right)^m\right)^2 & H_p < 0 \\ 1 & H_p \geq 0 \end{cases} \qquad (2)$$

$$Se = \begin{cases} \dfrac{1}{\left(1+\left|aH_p\right|^n\right)^m} & H_p < 0 \\ 1 & H_p \geq 0 \end{cases} \qquad (3)$$

$$\theta = \begin{cases} \theta_r + Se\left(\theta_s - \theta_r\right) & H_p < 0 \\ \theta_s & H_p \geq 0 \end{cases} \qquad (4)$$

$$m = 1 - \frac{1}{n} \qquad (5)$$

Liquid volume ranges from user-specified small residual value, θ_r, to the total porosity, θ_s. These bounds, as well as the constants a and n depend on material properties. The constant a (1/ft) is related to the air entry pressure head and desorption behavior of the soil, and n is related to the pore-size distribution of the soil. A detailed description of how these values were determined for the Hidden Dam model is provided below.

Determination of Variably Saturated Model Input Parameters

The model input parameters were obtained from the seepage studies conducted by Cedergren (1980a, b) and the Soil Plant Air Water (SPAW) soils database developed by Saxton and Rawls (2006) and available through the USDA-NRCS (*http://www.wsi.nrcs.usda.gov/products/W2Q/water_mgt/Water_Budgets/SPAW_Model.html*, last accessed January 2010). Estimates of the saturated hydraulic conductivity (table 1) and gradation curves (figure 47) corresponding to each sub-domain of the dam were provided by Cedergren (1980a) and the foundation report (U.S. Army Corps of Engineers, 1977). Grain size distributions were summarized in terms of percent gravel, sand, silt and clay, by employing a standardized grain scale.

Soil-water retention curves (figure 48) and saturated and residual moisture contents (table 1) for each sub-domain were estimated using the graphical user interface of Saxton and Rawls (2006) and the available gradation data. Percentages were entered into the SPAW database to obtain estimates of textural classification (table 1) and statistically based estimates of soil-water retention curves for each sub-domain. The retention curves relate matric suction ($H_p < 0$) to volumetric moisture content (volume fraction), and are a key component of the unsaturated flow models. Soil-water retention curves were created for matric suctions ranging between 1,500 kPa (31,328 lbf/ft^2), corresponding to absorbed soil moisture at the residual moisture condition, and atmospheric pressure, corresponding to soil moisture at the saturated condition. The curves

were produced under the assumption that the effects of organic matter and osmotic pressures were negligible. Soil compaction in the SPAW model was specified as "normal," implying that no unnatural changes in soil bulk density had occurred.

Table 2. Summary of gradation and soil-water retention data for Hidden Dam model units.

	Impervious Core	Random Fill	Select Fill	Drainage Fill
Saturated hydraulic conductivity (ft/day)	0.02	1.0	2.0	8000.0
Gravel (weight fraction)	0.10	0.25	0.30	1.00
Sand (weight fraction)	0.45	0.10	0.50	0.00
Silt (weight fraction)	0.10	0.63	0.18	0.00
Clay (weight fraction)	0.35	0.02	0.02	0.00
Textural classification	Sandy clay	Silty loam	Sandy loam	Sandy gravel
Residual moisture (volume fraction)	0.21	0.02	0.01	0.02
Saturated moisture (volume fraction)	0.42	0.37	0.38	0.43
a (1/ft)	0.2013	0.2399	0.2453	0.7165
n	1.9923	3.9218	3.3088	3.5952

The soil-water retention curves are incorporated into the flow model by determining the parameters a and n in equations (3) and (4) that fit each retention curve produced by the SPAW model. These parameters define the relative permeability as a function of saturation in equation (2), which is incorporated in the variably saturated flow equation (1). Nominal values a = 0.2 / ft and n = 2.0 are used for the grout curtain and bedrock as the necessary input parameters were not available for these units.

Electrokinetic Coupling to Determine the Self-Potential Response

Electrokinetic coupling is the mechanism by which fluid flow in porous media generates measurable electrical potentials in the earth, called self-potentials (Ishido and Mizutani, 1981; Morgan and others, 1989; Revil and others, 1999). The basic concept, summarized by Minsley and others (2010), involves a small amount of excess positive charge that is transported along with fluid flow in porous materials, generating a "streaming" electric current density. Because the total electric current density in the earth must be conserved, this streaming current density generates a balancing conduction current density that flows throughout the earth. As this conduction current traverses the subsurface electrical resistivity structure, it results in measurable electrical potential differences between various locations, which are called self-potentials.

Mathematically, this phenomenon is written

$$\nabla \cdot \left(j_s + j_c \right) = \nabla \cdot \left(Q_V u - \sigma \nabla V \right) = 0 \qquad (6)$$

where j_s and j_c represent the streaming and conduction currents (A/ft^2), respectively. The streaming current can be defined as the excess charge density Q_V in coulombs per cubic foot (C/ft^3) times the fluid velocity u (ft/s). The conduction current is defined as the negative of the electrical conductivity (S/m) times the electrical potential gradient (V/ft). The difference in electrical potential, V, between two locations is the self-potential value (V). By

coupling the electrical problem to the variably saturated flow problem, the self-potential response can be calculated for any flow scenario.

Equation (6) can be solved in COMSOL by coupling directly to the flow velocity, u, that is calculated in the solution of Richards equation discussed previously. The subsurface electrical conductivity structure (σ) is calculated dynamically as a function of the liquid volume content, θ, in equation (4) using Archie's law (Archie, 1942; Lesmes and Friedman, 2005),

$$\sigma = \sigma_w \theta^m \qquad (7)$$

where σ_w is the electrical conductivity of the pore water, and is fixed at a value of 0.05 S/m (20 ohm-m) for this study. The cementation exponent, m, is fixed at 1.7. An example of the electrical resistivity (inverse of conductivity) structure for one flow model is shown in figure 12. The excess charge density, Q_V, is also calculated dynamically as a function of the saturation-dependent hydraulic permeability, k, using the relationship provided by Jardani and others (2008):

$$\log(Q_V) = -9.2349 - 0.8219 \log(k) \qquad (8)$$

Figures

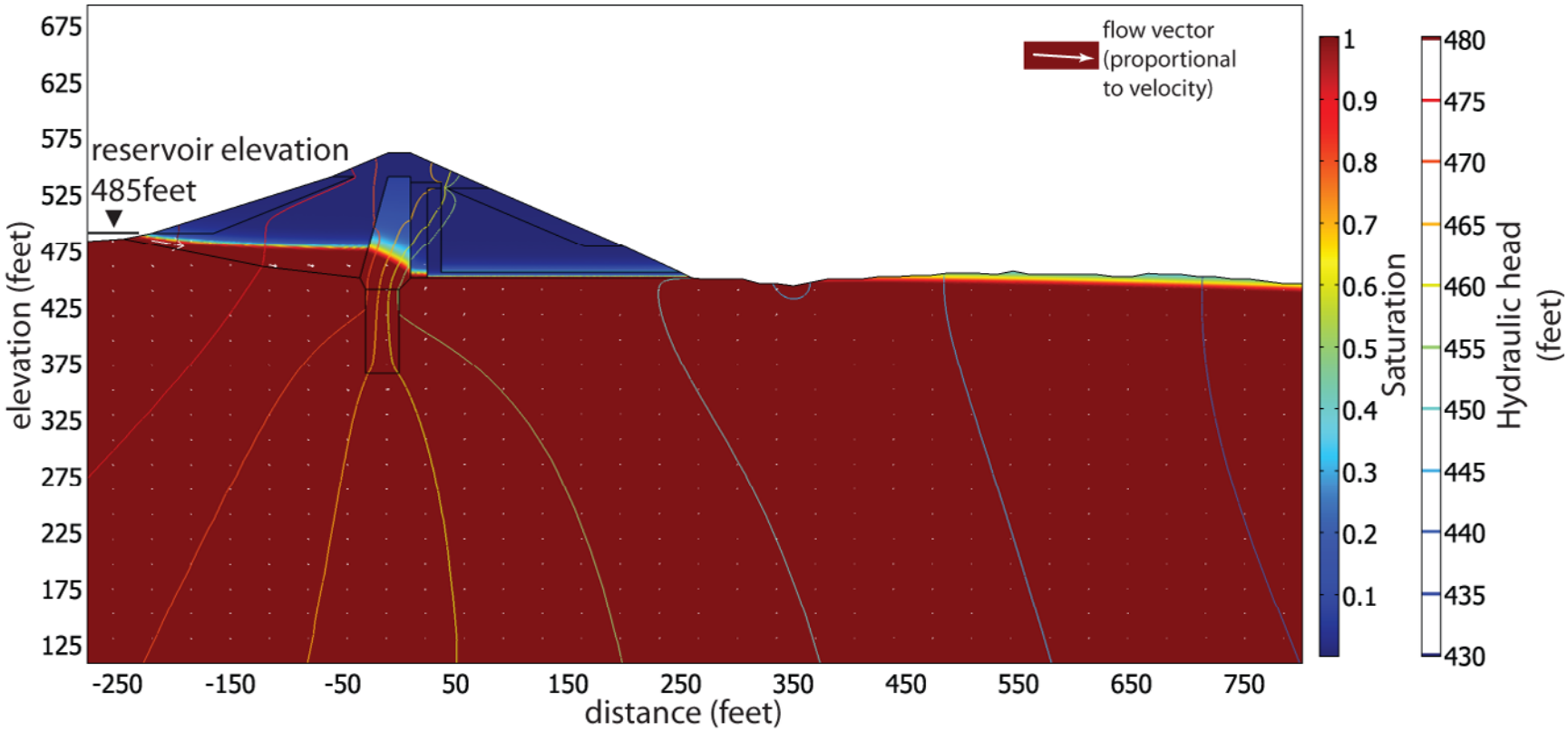

Figure 5. Flow model results for the profile A baseline model and reservoir elevation of 485 ft (flow scenario 1). Background colors represent the effective saturation, contours indicate hydraulic head (feet), and white arrows show flow directions and relative magnitude.

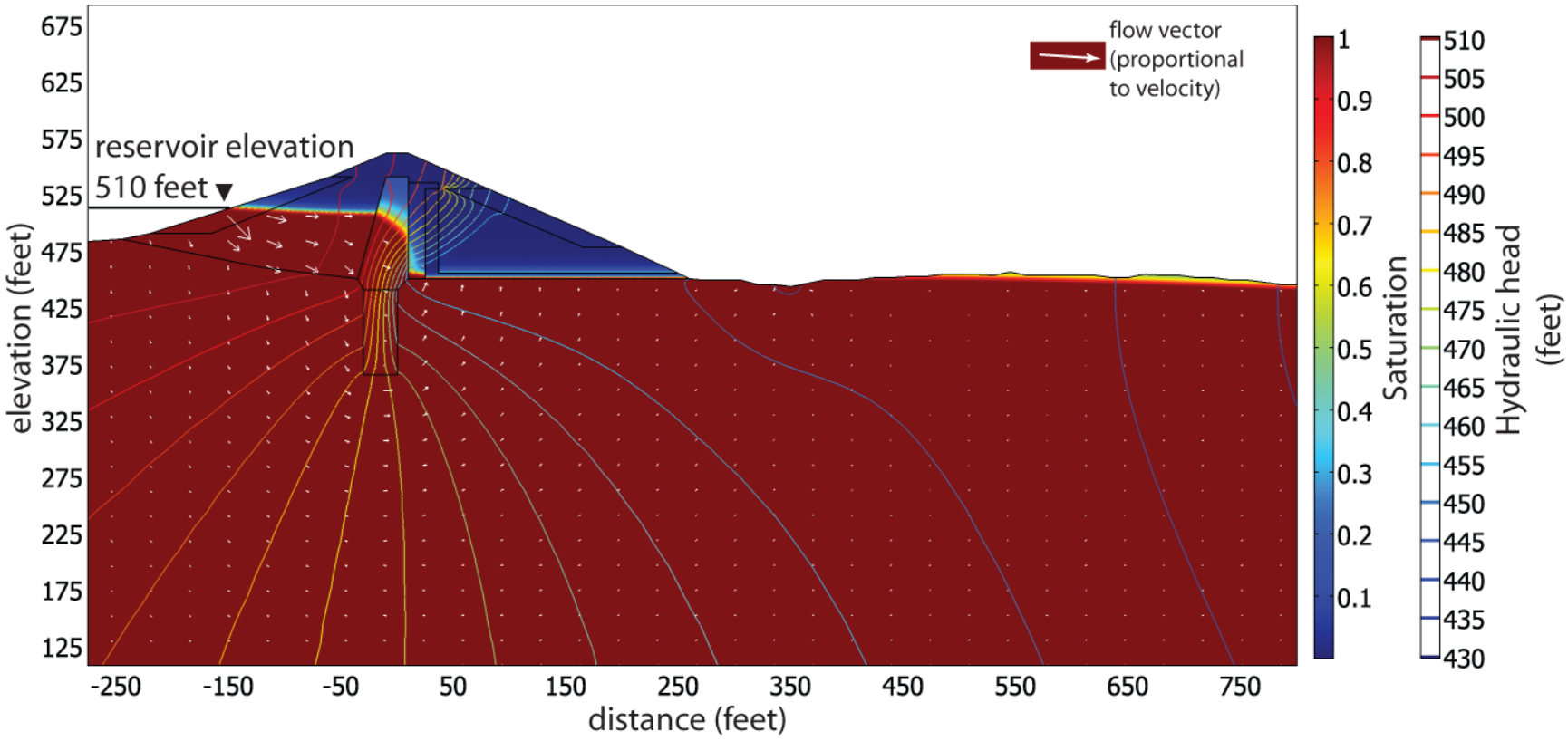

Figure 6. Flow model results for the profile A baseline model and reservoir elevation of 510 ft (flow scenario 1). Background colors represent the effective saturation, contours indicate hydraulic head (feet), and white arrows show flow directions and relative magnitude.

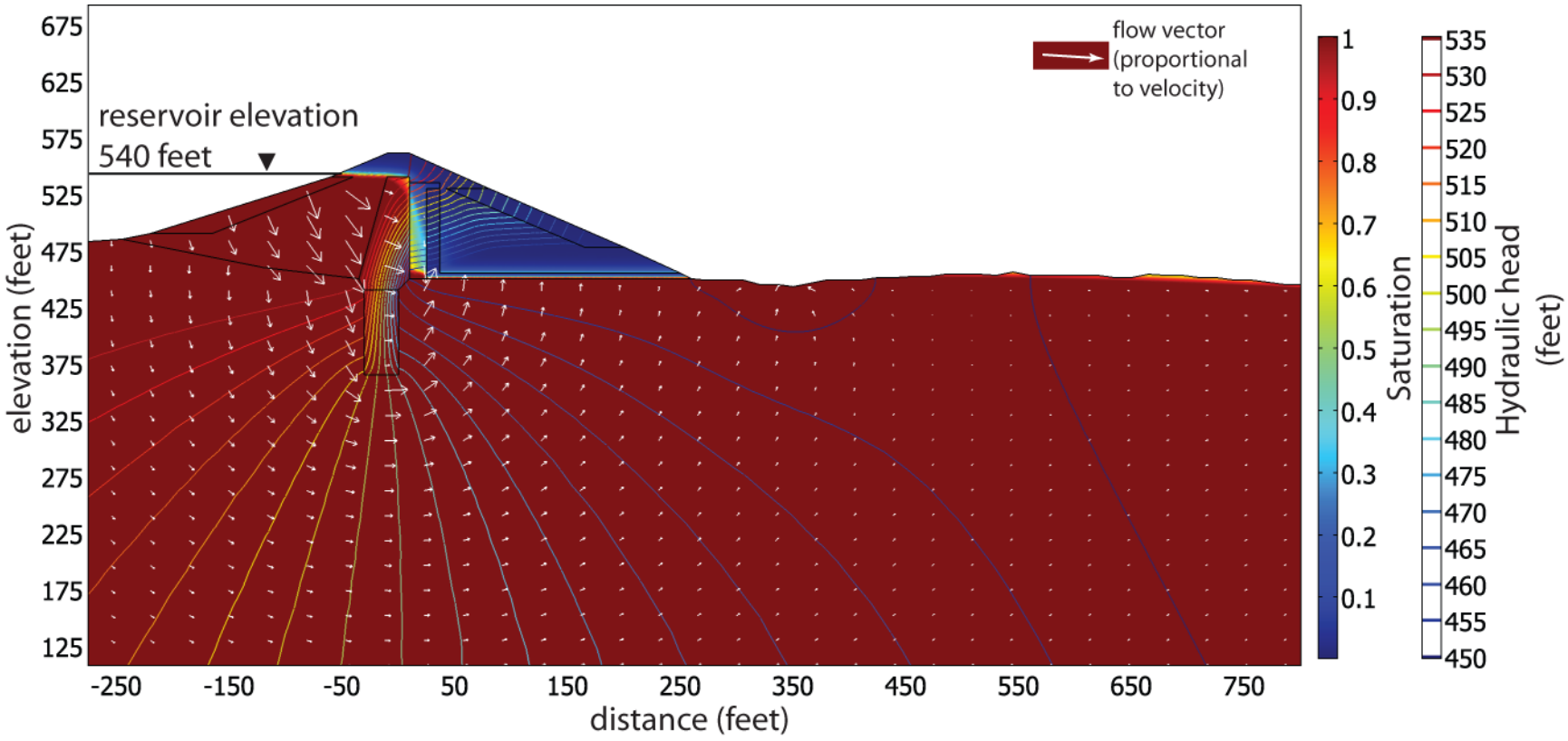

Figure 7. Flow model results for the profile A baseline model and reservoir elevation of 540 ft (flow scenario 1). Background colors represent the effective saturation, contours indicate hydraulic head (feet), and white arrows show flow directions and relative magnitude.

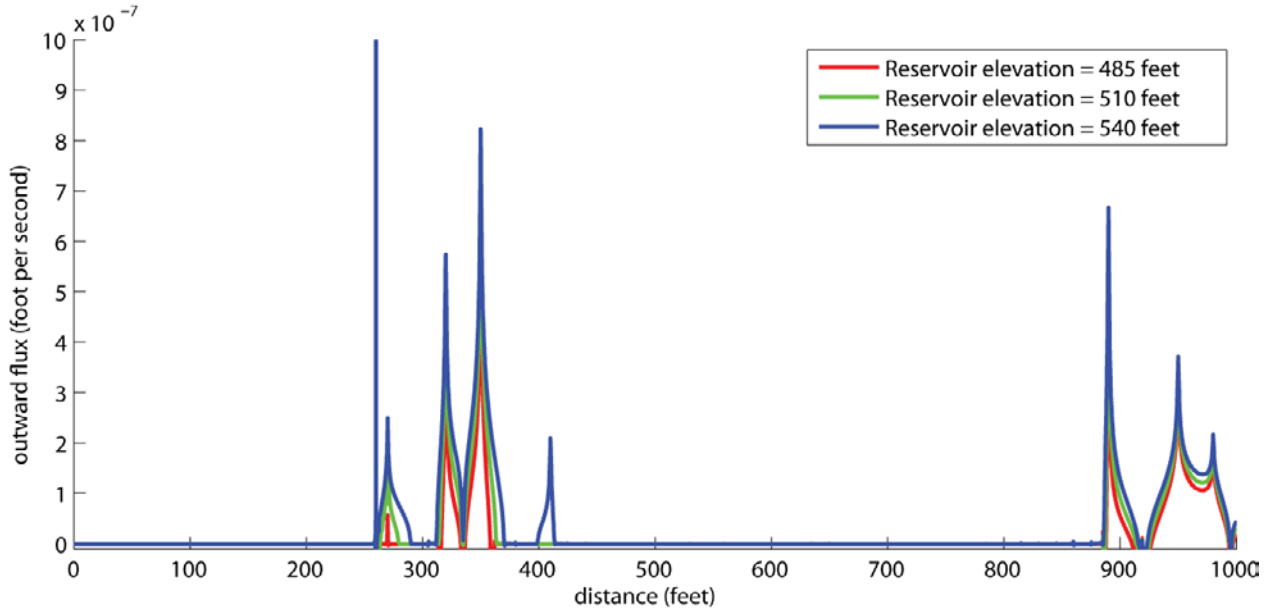

Figure 8. Seepage (foot per second) through the downstream embankment and ground surface as a function of distance for the three different reservoir elevations illustrated in figure 5–7 (flow scenario 1).

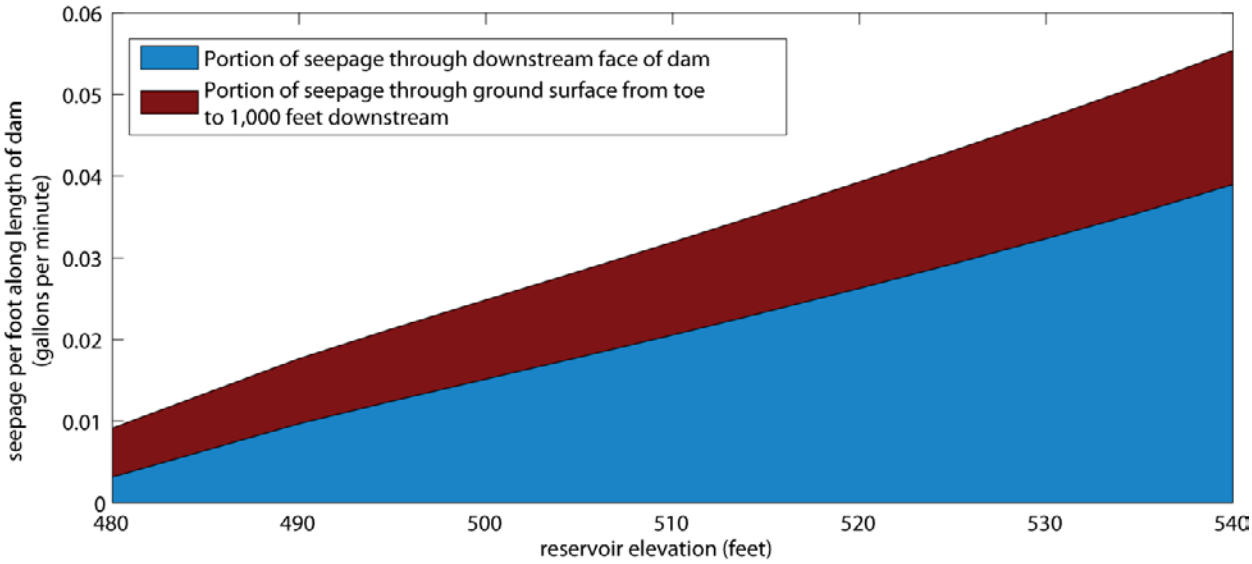

Figure 9. Volumetric flow (gallons per minute) through the downstream embankment (blue) and ground surface (red) per foot along the length of the dam as a function of reservoir elevation (flow scenario 1).

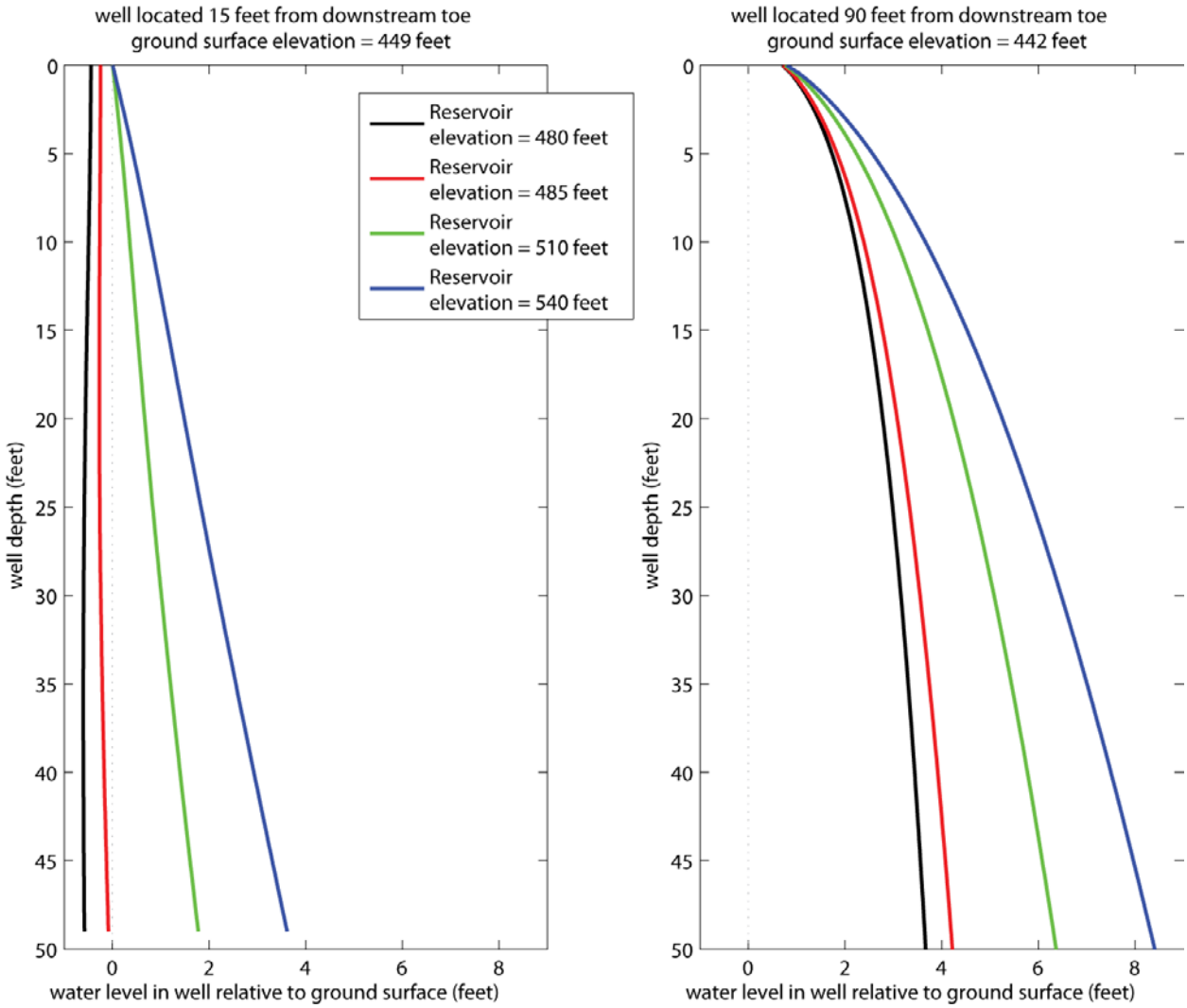

Figure 10. Predicted water levels in observation wells 15 feet (left) and 90 feet (right) from the downstream toe for flow scenario 1. The predicted water level relative to ground surface (positive upwards) is shown for different reservoir elevations and any well depth between 0 and 50 feet.

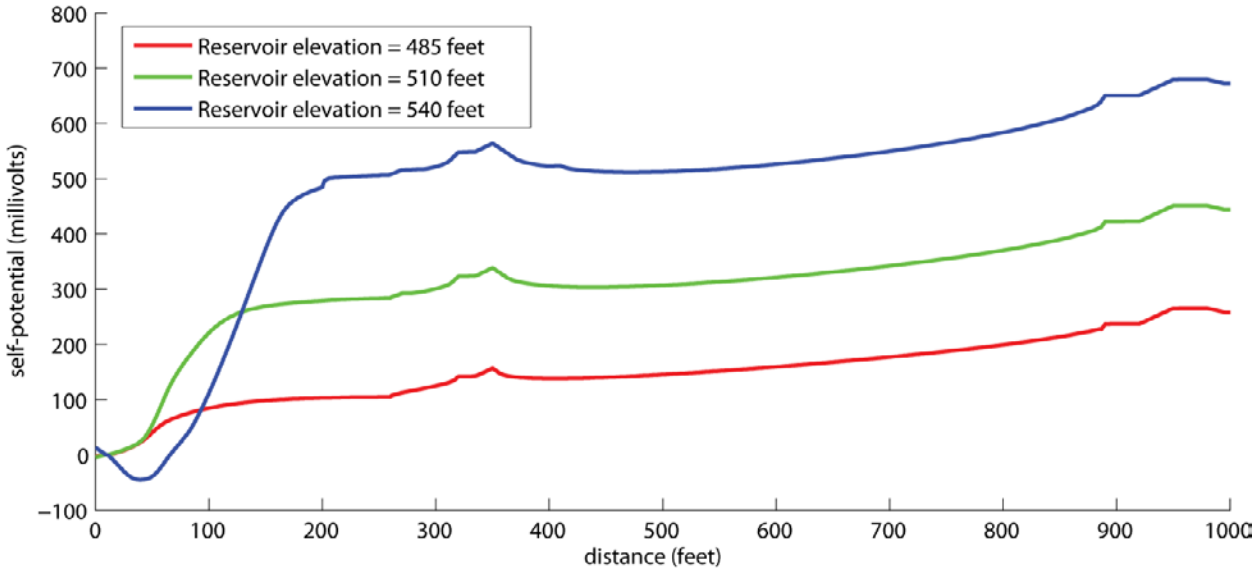

Figure 11. Self-potential (millivolts) values predicted along the downstream embankment and ground surface for the three different reservoir elevations illustrated in figure 5–7 for flow scenario 1.

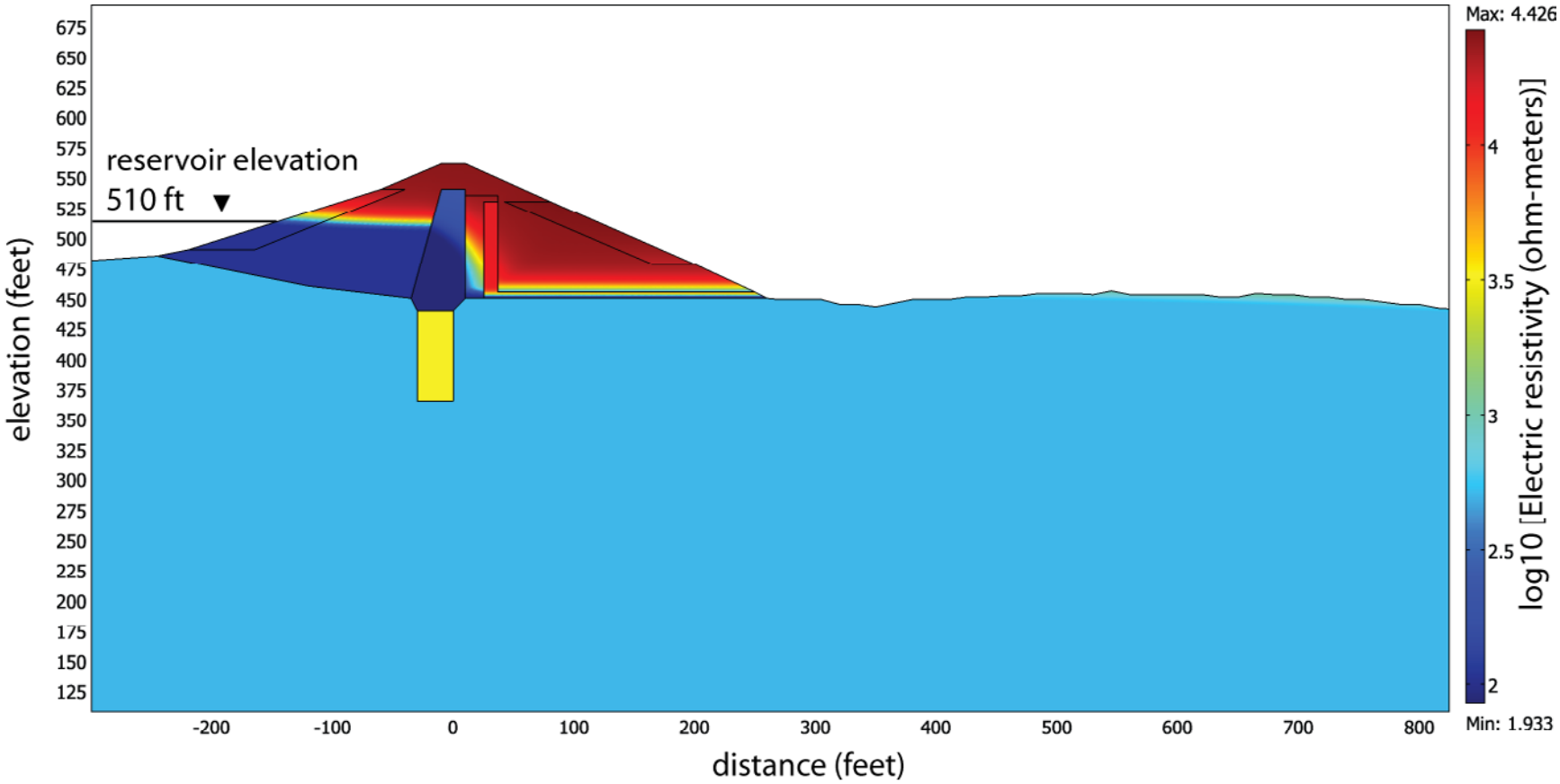

Figure 12. Electrical resistivity (ohm-meters) predicted for flow scenario 1 at a reservoir elevation of 510 feet.

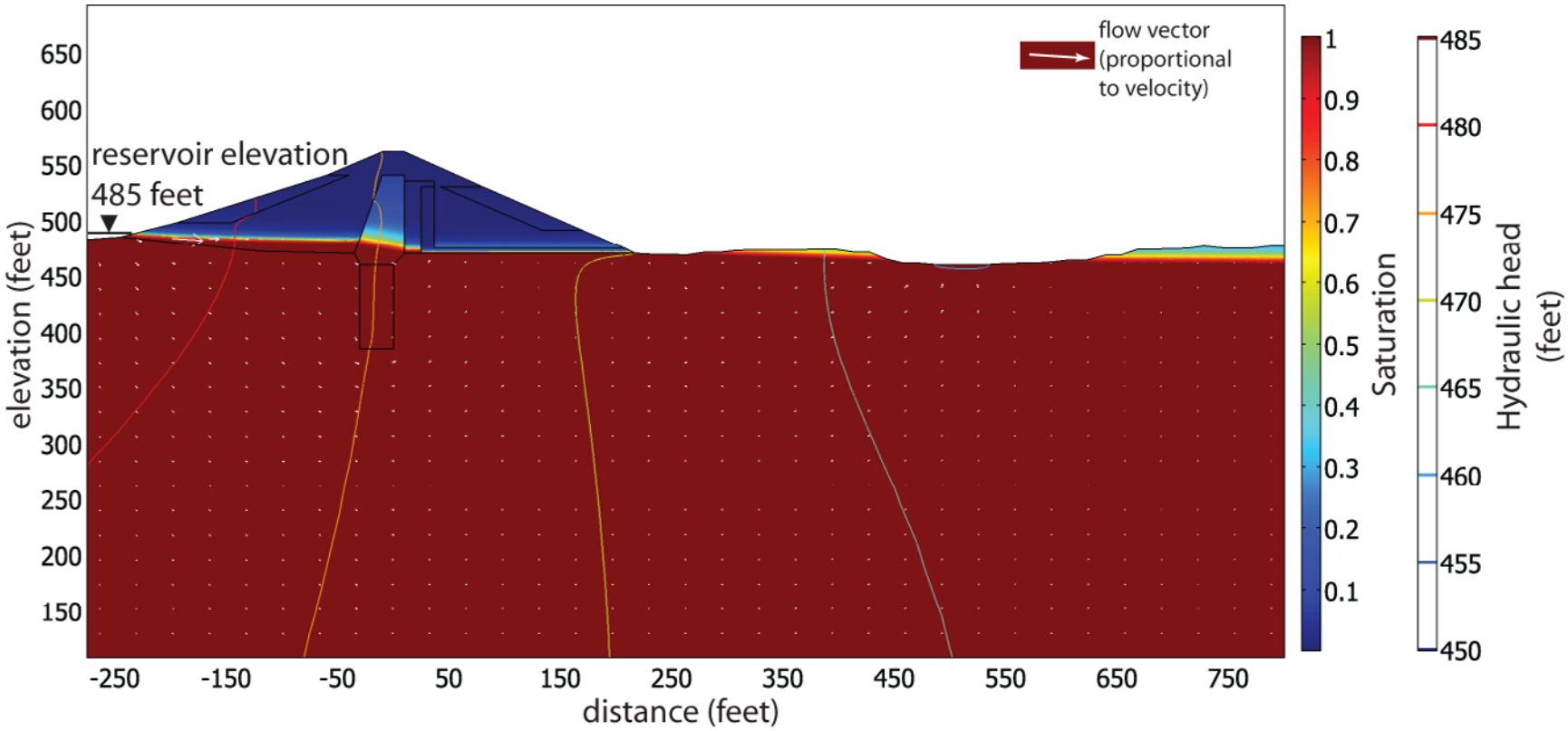

Figure 13. Flow model results for the profile B baseline model and reservoir elevation of 485 ft (flow scenario 2). Background colors represent the effective saturation, contours indicate hydraulic head (feet), and white arrows show flow directions and relative magnitude.

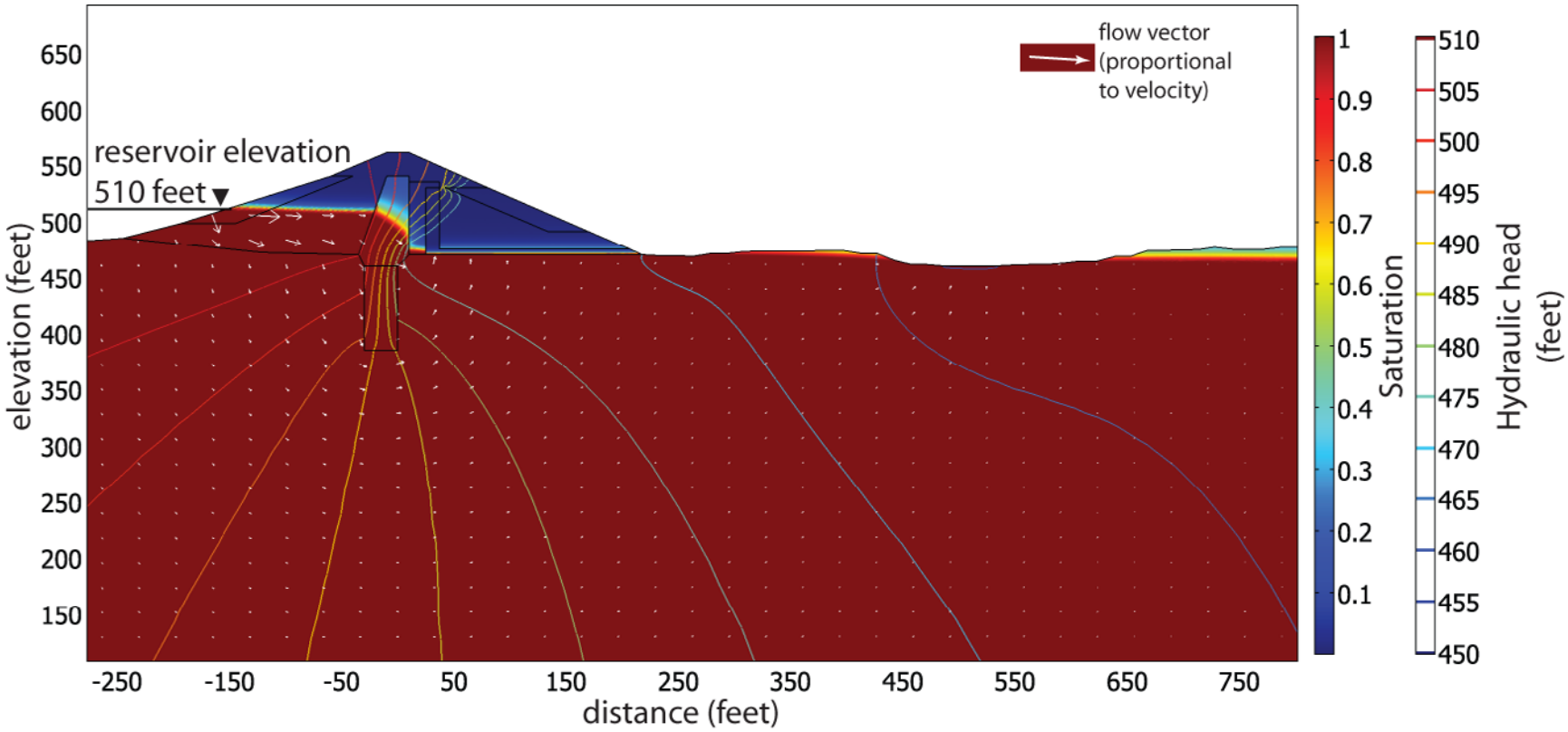

Figure 14. Flow model results for the profile B baseline model and reservoir elevation of 510 ft (flow scenario 2). Background colors represent the effective saturation, contours indicate hydraulic head (feet), and white arrows show flow directions and relative magnitude.

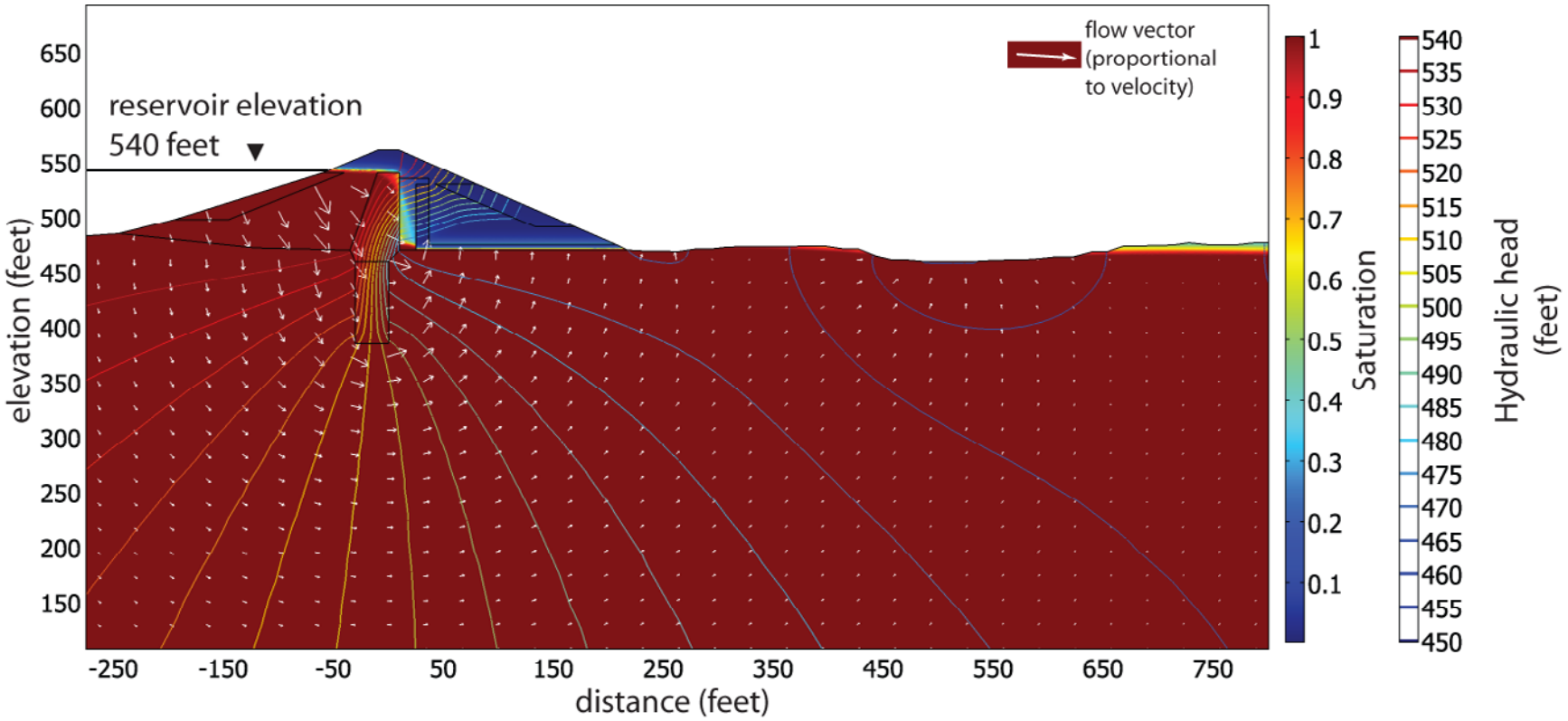

Figure 15. Flow model results for the profile B baseline model and reservoir elevation of 540 ft (flow scenario 2). Background colors represent the effective saturation, contours indicate hydraulic head (feet), and white arrows show flow directions and relative magnitude.

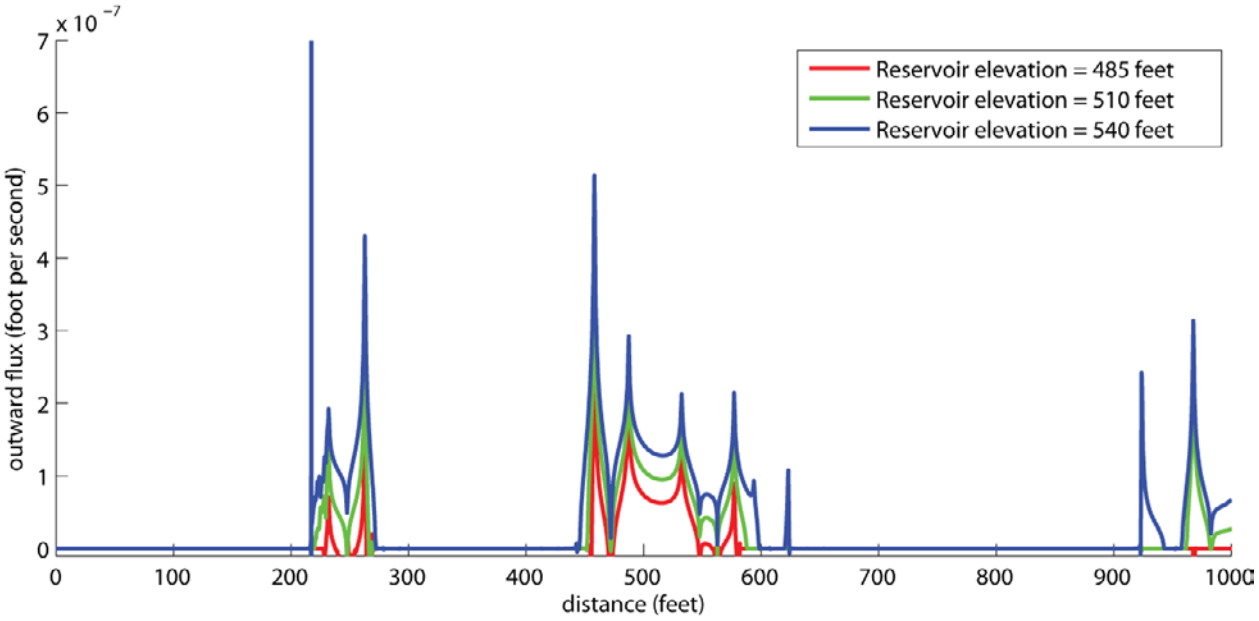

Figure 16. Seepage (foot per second) through the downstream embankment and ground surface as a function of distance for the three different reservoir elevations illustrated in figure 13–15 (flow scenario 2).

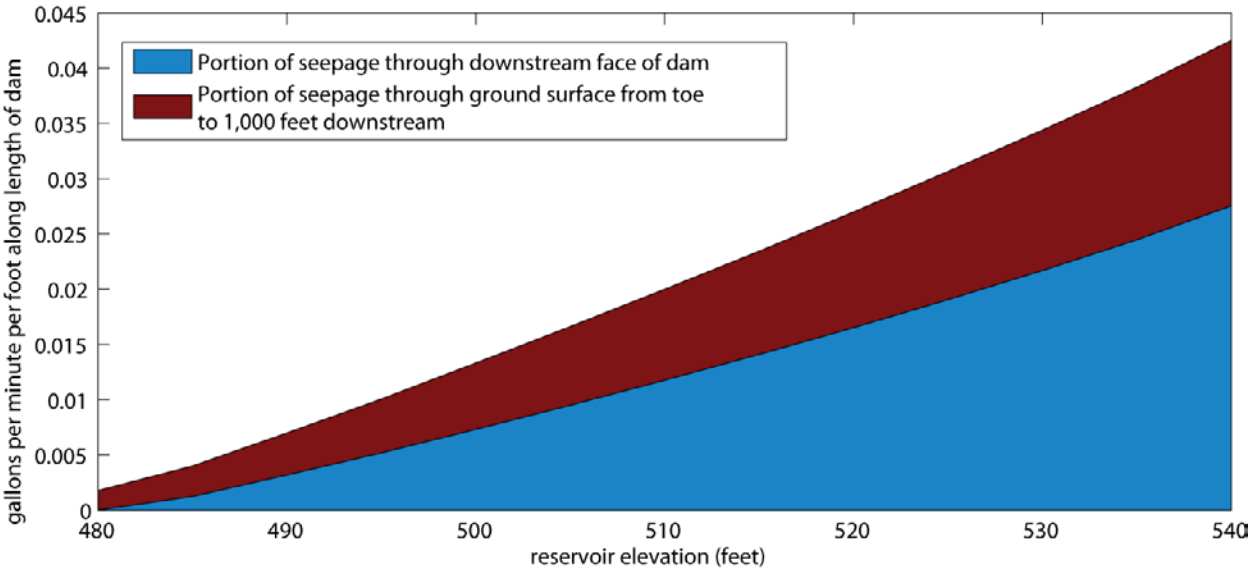

Figure 17. Volumetric flow (gallons per minute) through the downstream embankment (blue) and ground surface (red) per foot along the length of the dam as a function of reservoir elevation for flow scenario 2.

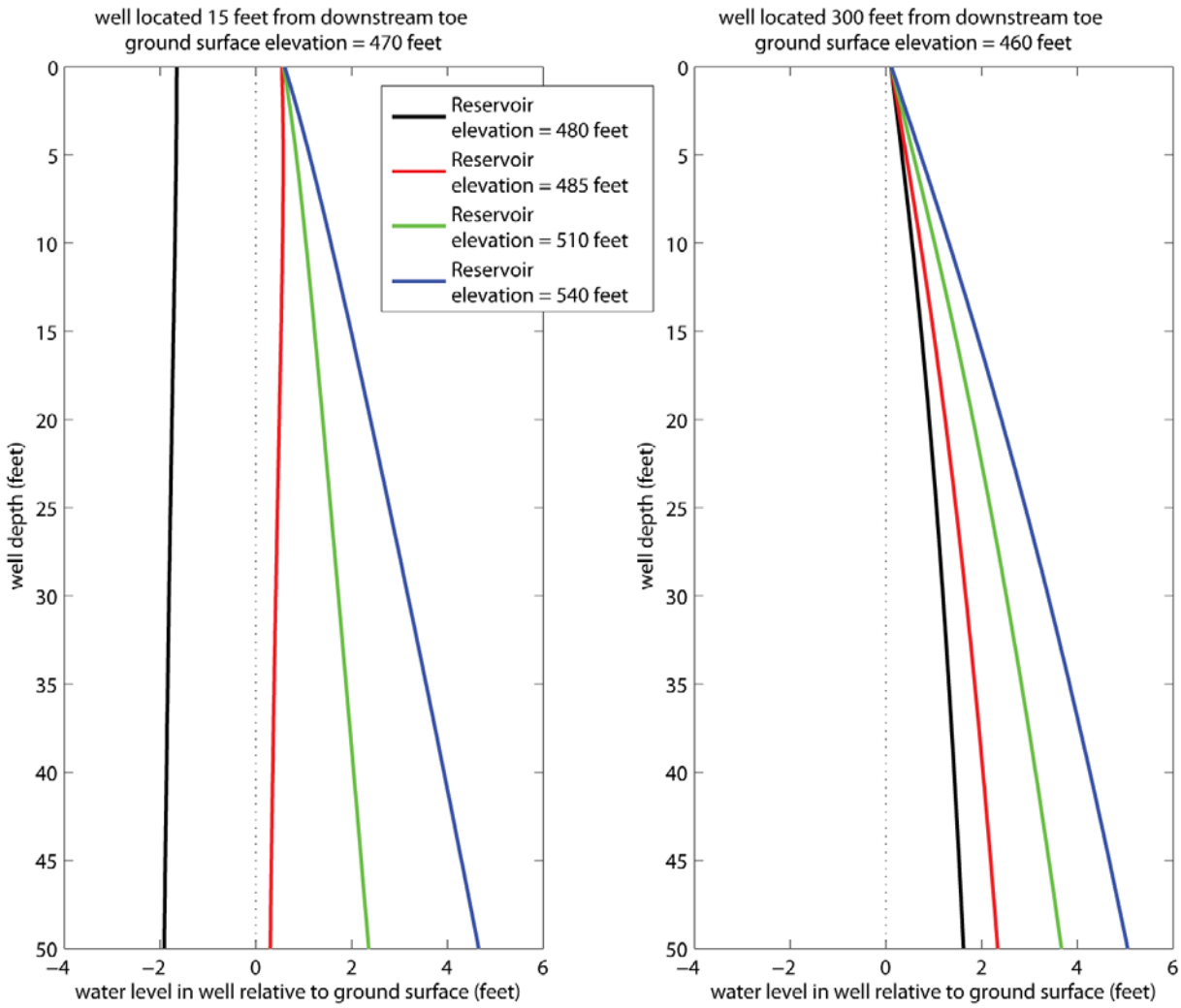

Figure 18. Predicted water levels in observation wells 15 feet (left) and 300 feet (right) from the downstream toe for flow scenario 2. The predicted water level relative to ground surface (positive upwards) is shown for different reservoir elevations and any well depth between 0 and 50 feet.

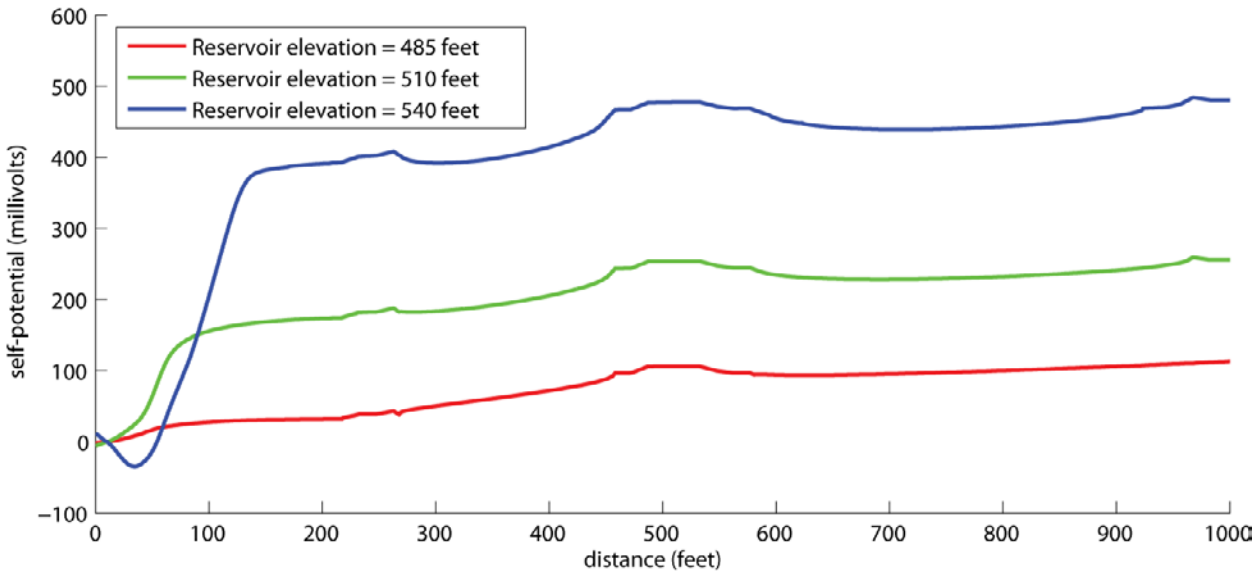

Figure 19. Self-potential (millivolts) values predicted along the downstream embankment and ground surface for the three different reservoir elevations illustrated in figure 13–15 for flow scenario 2.

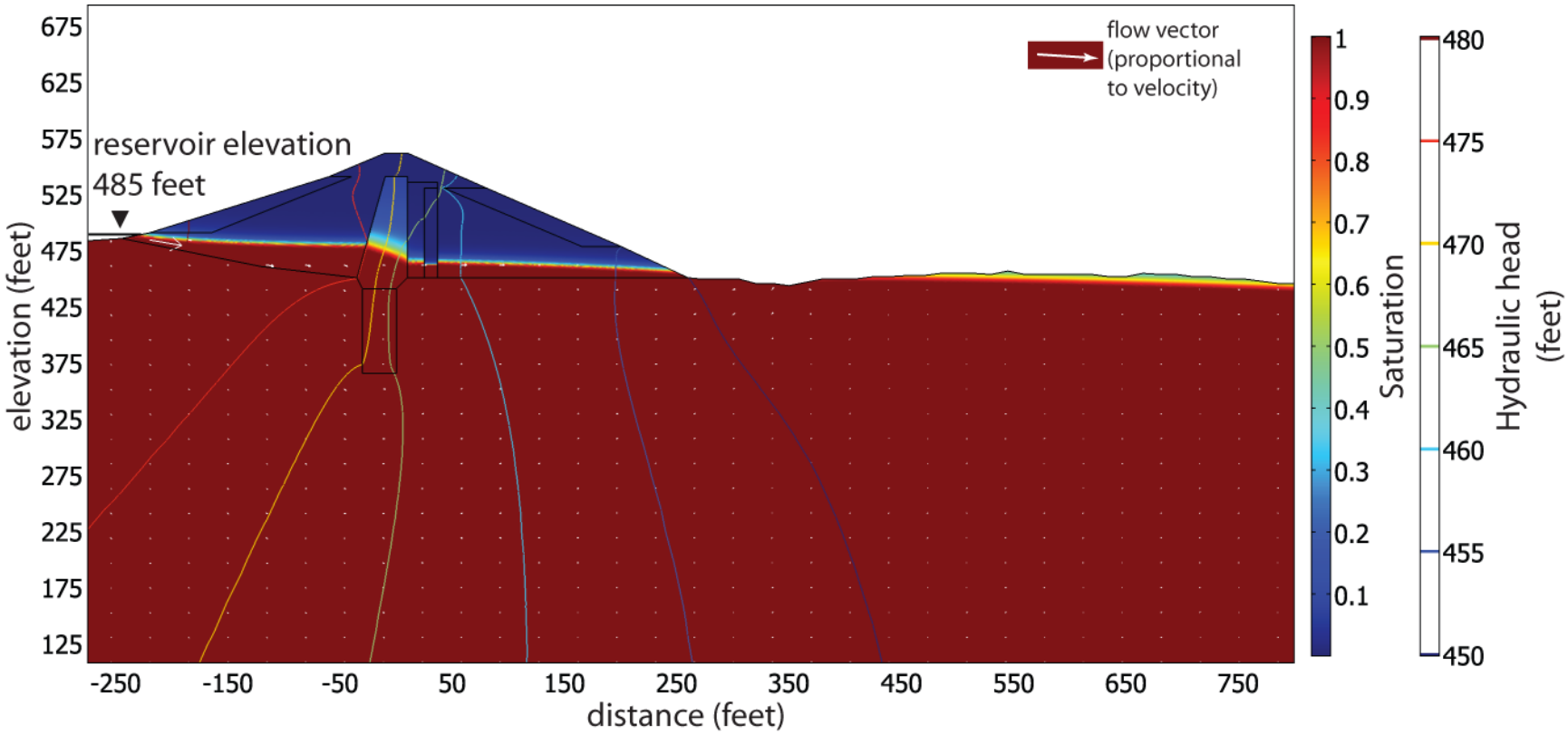

Figure 20. Flow model results for the profile A model with no horizontal-drainage fill and reservoir elevation of 485 ft (flow scenario 3). Background colors represent the effective saturation, contours indicate hydraulic head (feet), and white arrows show flow directions and relative magnitude.

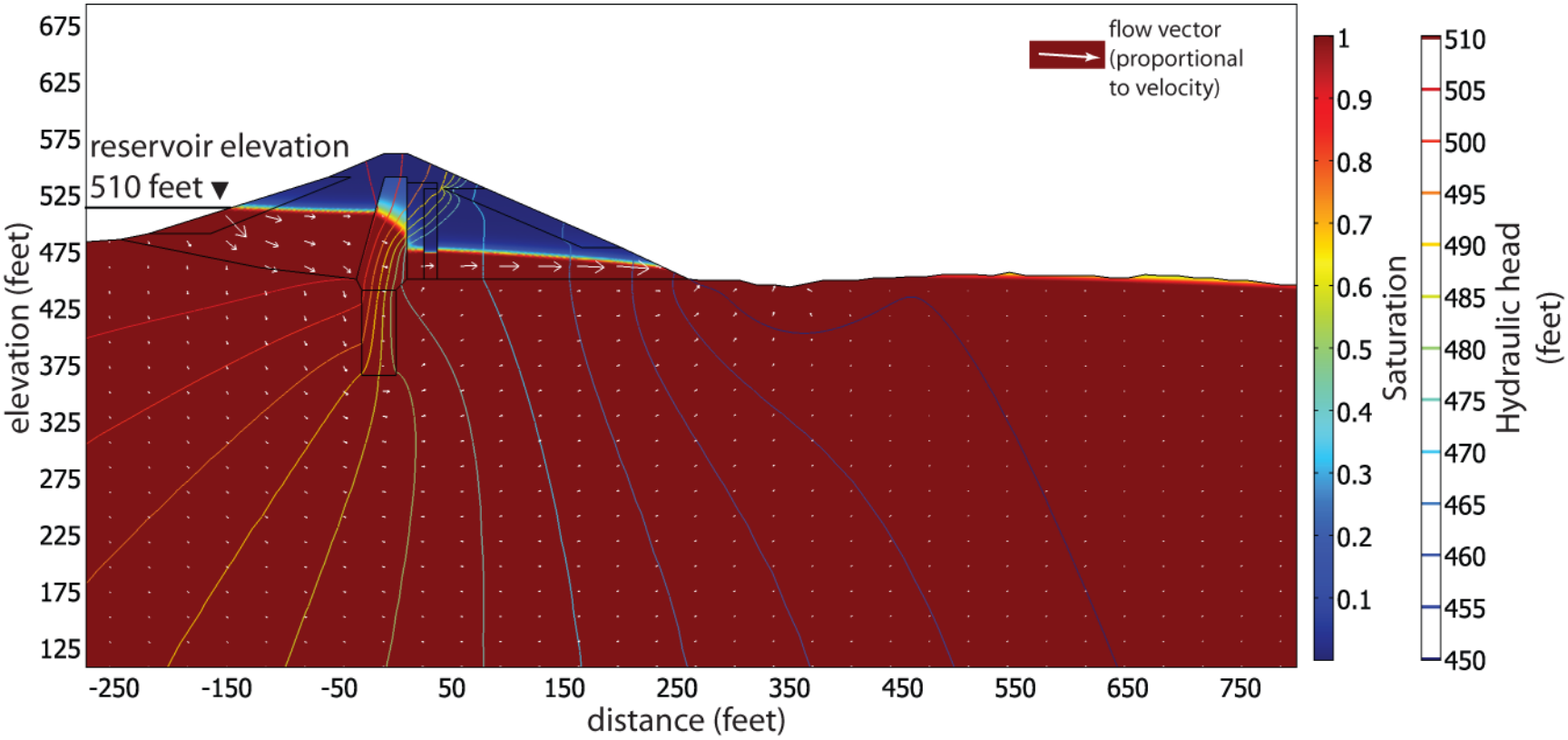

Figure 21. Flow model results for the profile A model with no horizontal-drainage fill and reservoir elevation of 510 ft (flow scenario 3). Background colors represent the effective saturation, contours indicate hydraulic head (feet), and white arrows show flow directions and relative magnitude.

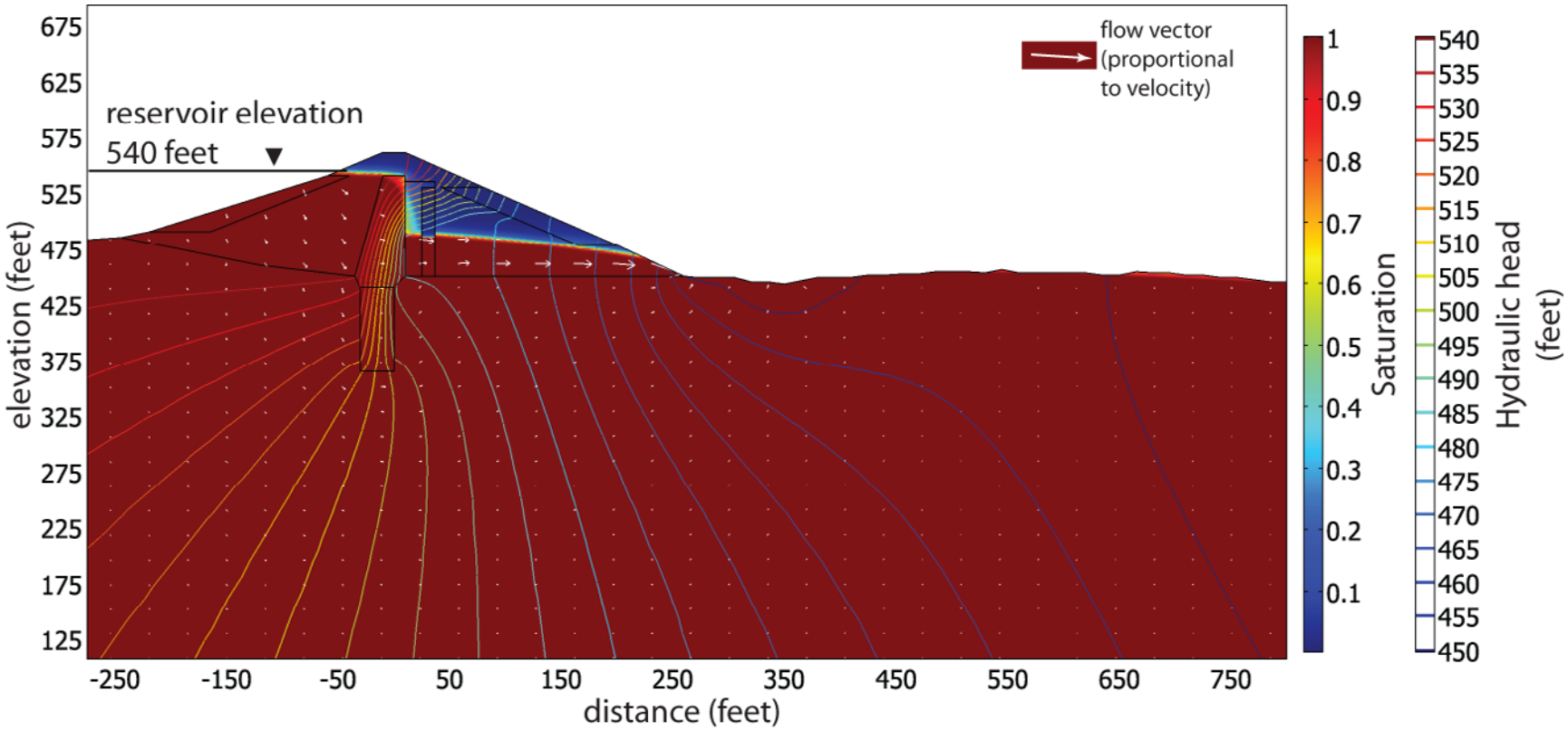

Figure 22. Flow model results for the profile A model with no horizontal-drainage fill and reservoir elevation of 540 ft (flow scenario 3). Background colors represent the effective saturation, contours indicate hydraulic head (feet), and white arrows show flow directions and relative magnitude.

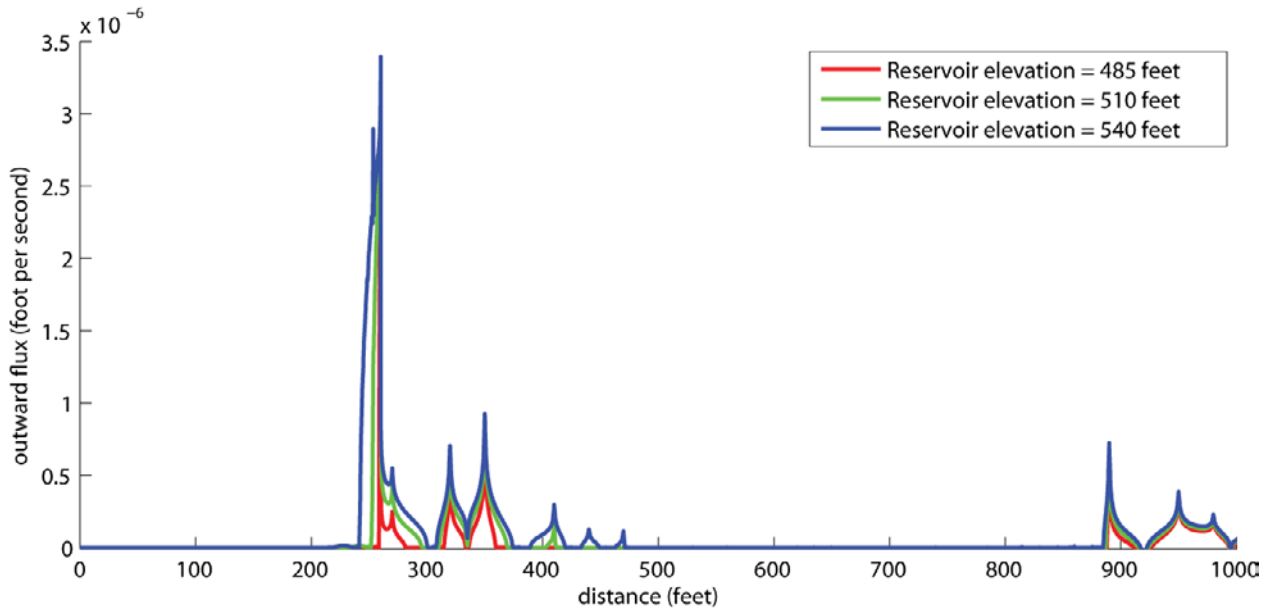

Figure 23. Seepage (foot per second) through the downstream embankment and ground surface as a function of distance for the three different reservoir elevations illustrated in figure 20–22 (flow scenario 3).

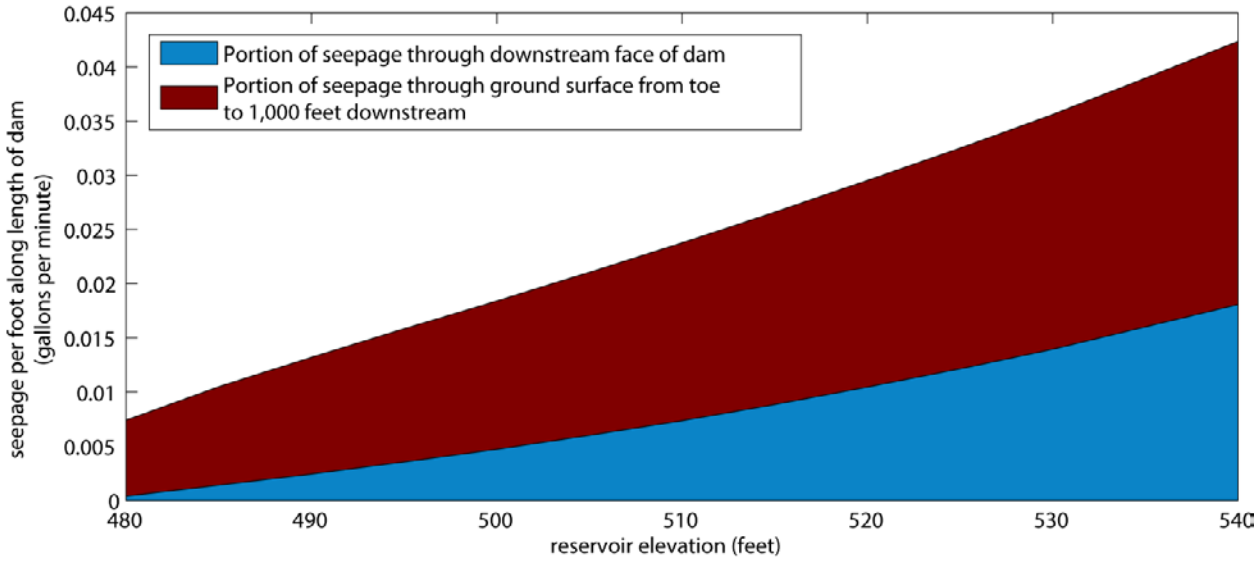

Figure 24. Volumetric flow (gallons per minute) through the downstream embankment (blue) and ground surface (red) per foot along the length of the dam as a function of reservoir elevation for flow scenario 3.

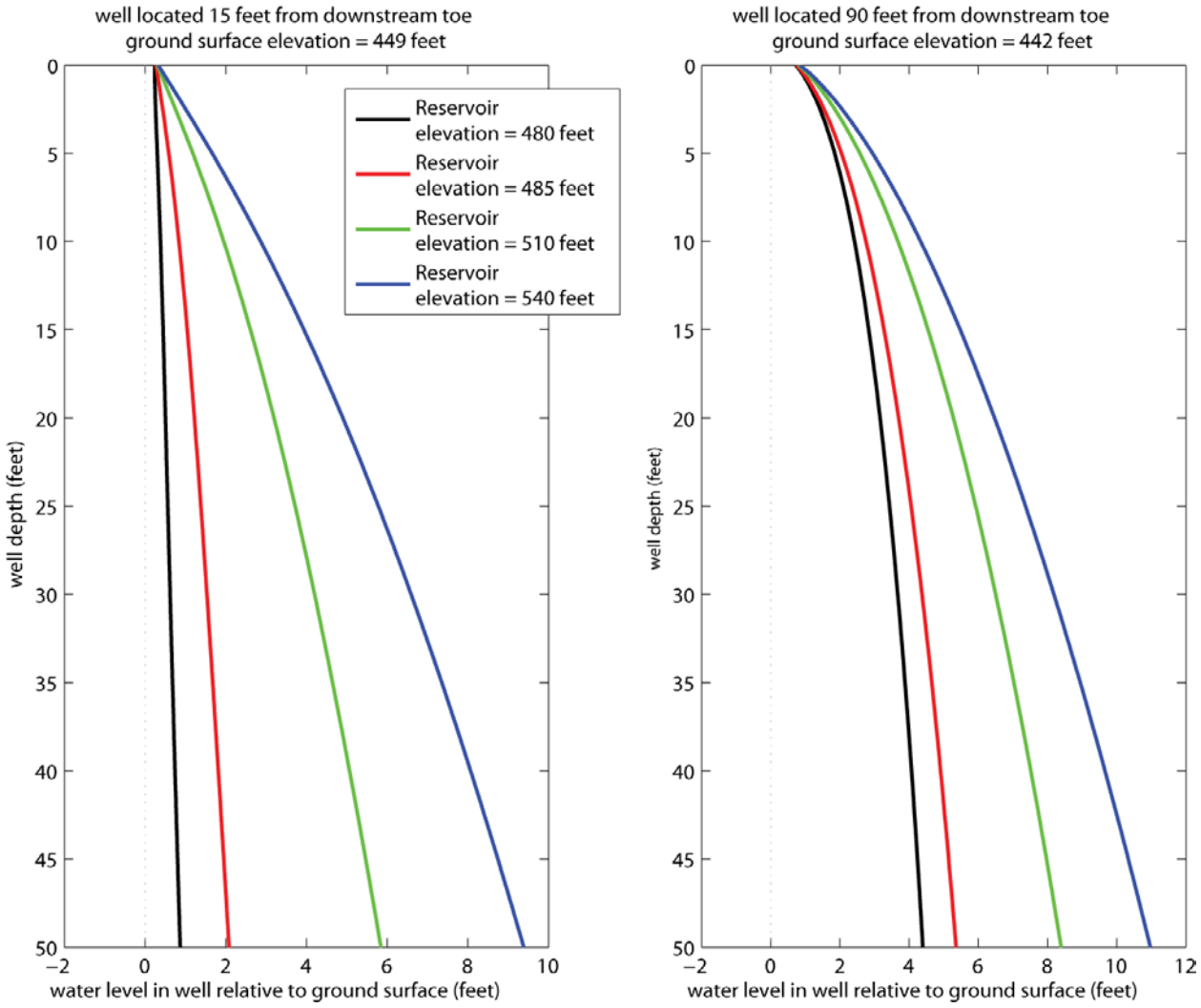

Figure 25. Predicted water levels in observation wells 15 feet (left) and 90 feet (right) from the downstream toe for flow scenario 3. The predicted water level relative to ground surface (positive upwards) is shown for different reservoir elevations and any well depth between 0 and 50 feet.

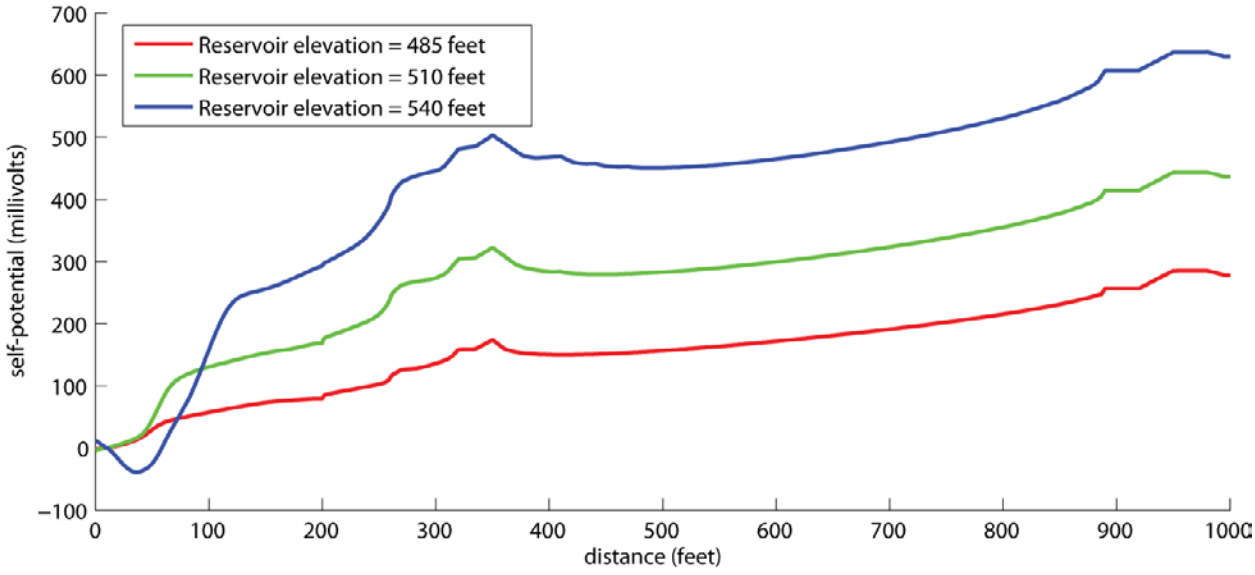

Figure 26. Self-potential (millivolts) values predicted along the downstream embankment and ground surface for the three different reservoir elevations illustrated in figure 20–22 for flow scenario 3.

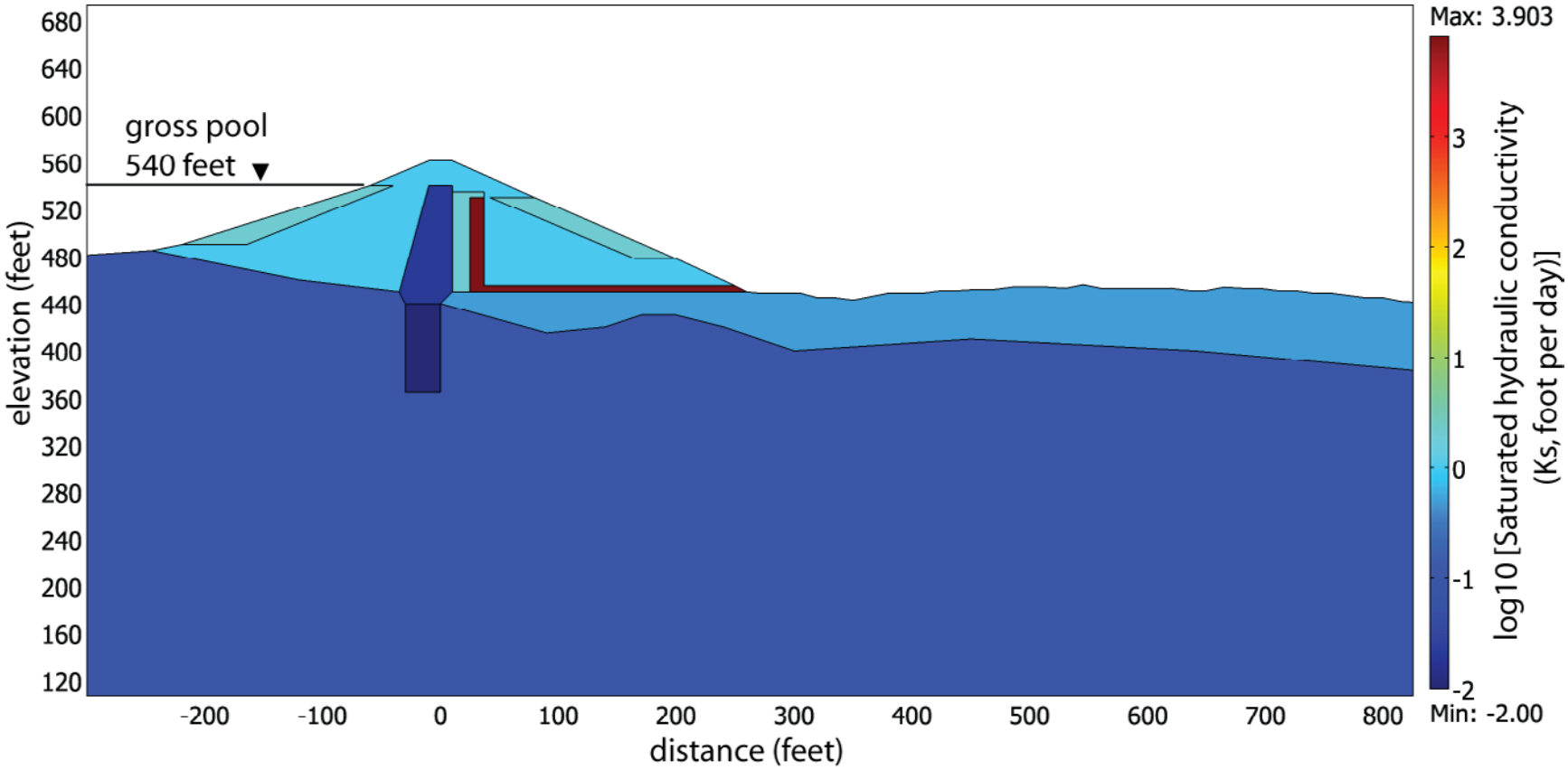

Figure 27. Saturated hydraulic-conductivity values for scenario 4 are identical to scenario 1 (figure 3), with the addition of a higher conductivity near-surface layer in the downstream portion of the model.

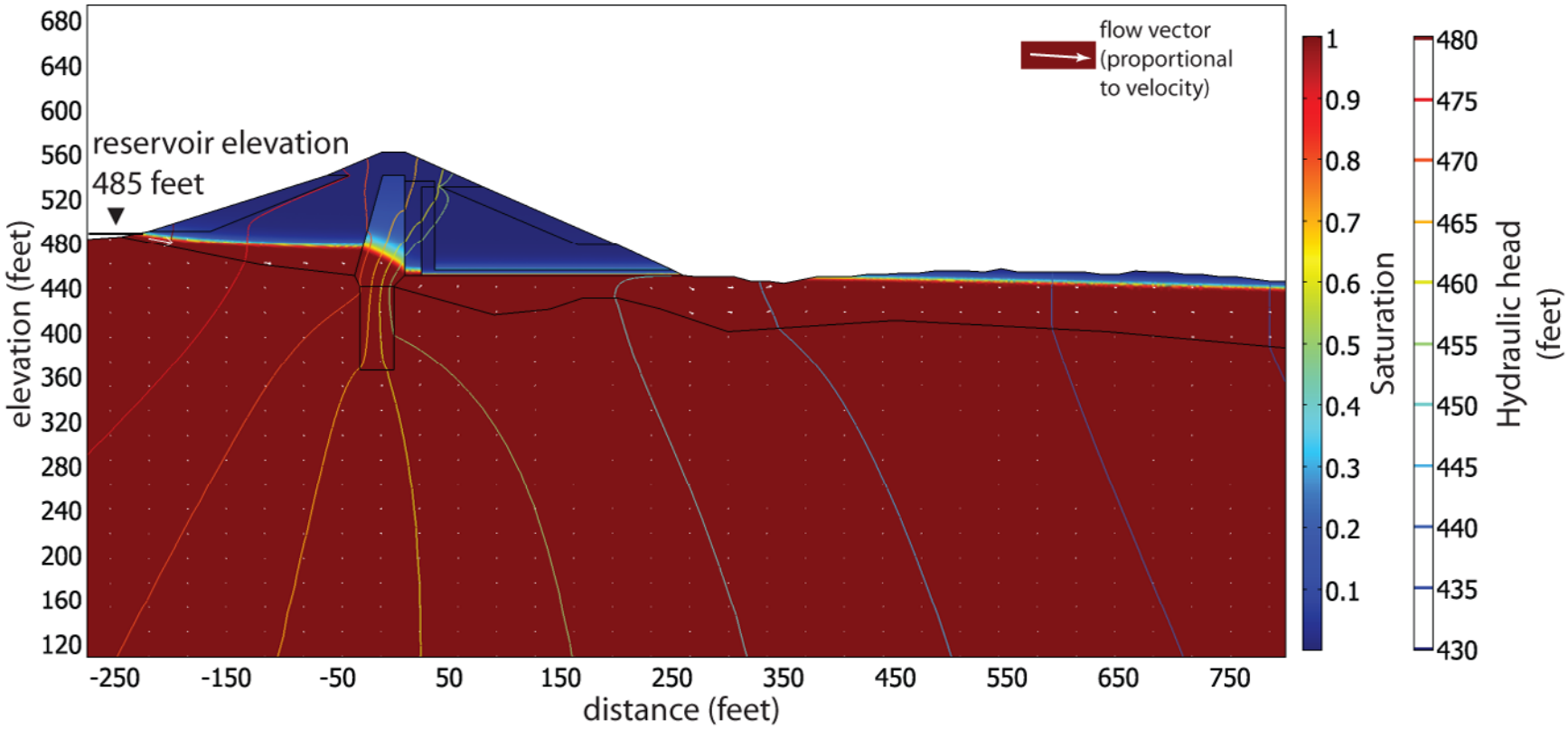

Figure 28. Flow model results for the profile A baseline model with an additional near-surface sediment layer and reservoir elevation of 485 ft (flow scenario 4). Background colors represent the effective saturation, contours indicate hydraulic head (feet), and white arrows show flow directions and relative magnitude.

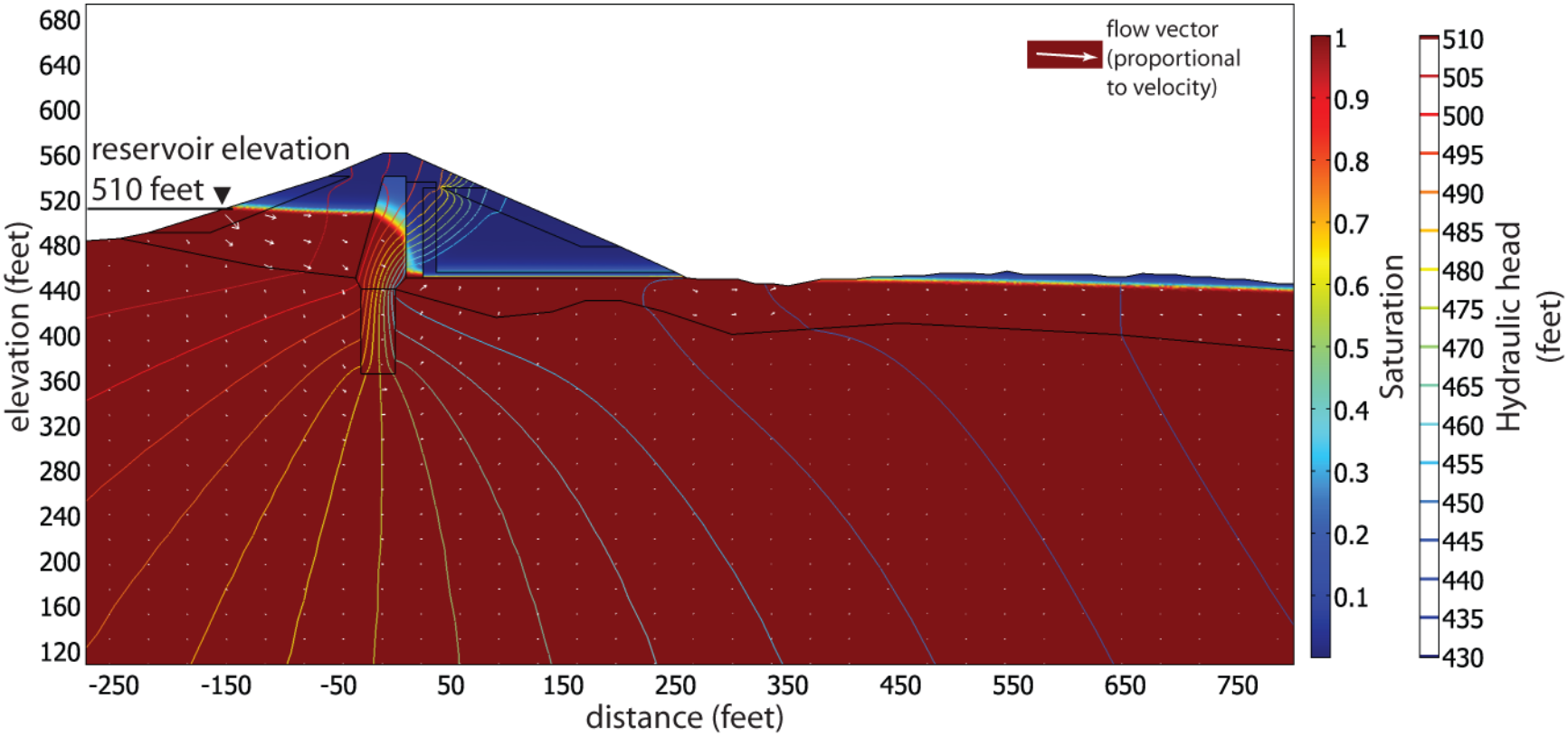

Figure 29. Flow model results for the profile A baseline model with an additional near-surface sediment layer and reservoir elevation of 510 ft (flow scenario 4). Background colors represent the effective saturation, contours indicate hydraulic head (feet), and white arrows show flow directions and relative magnitude.

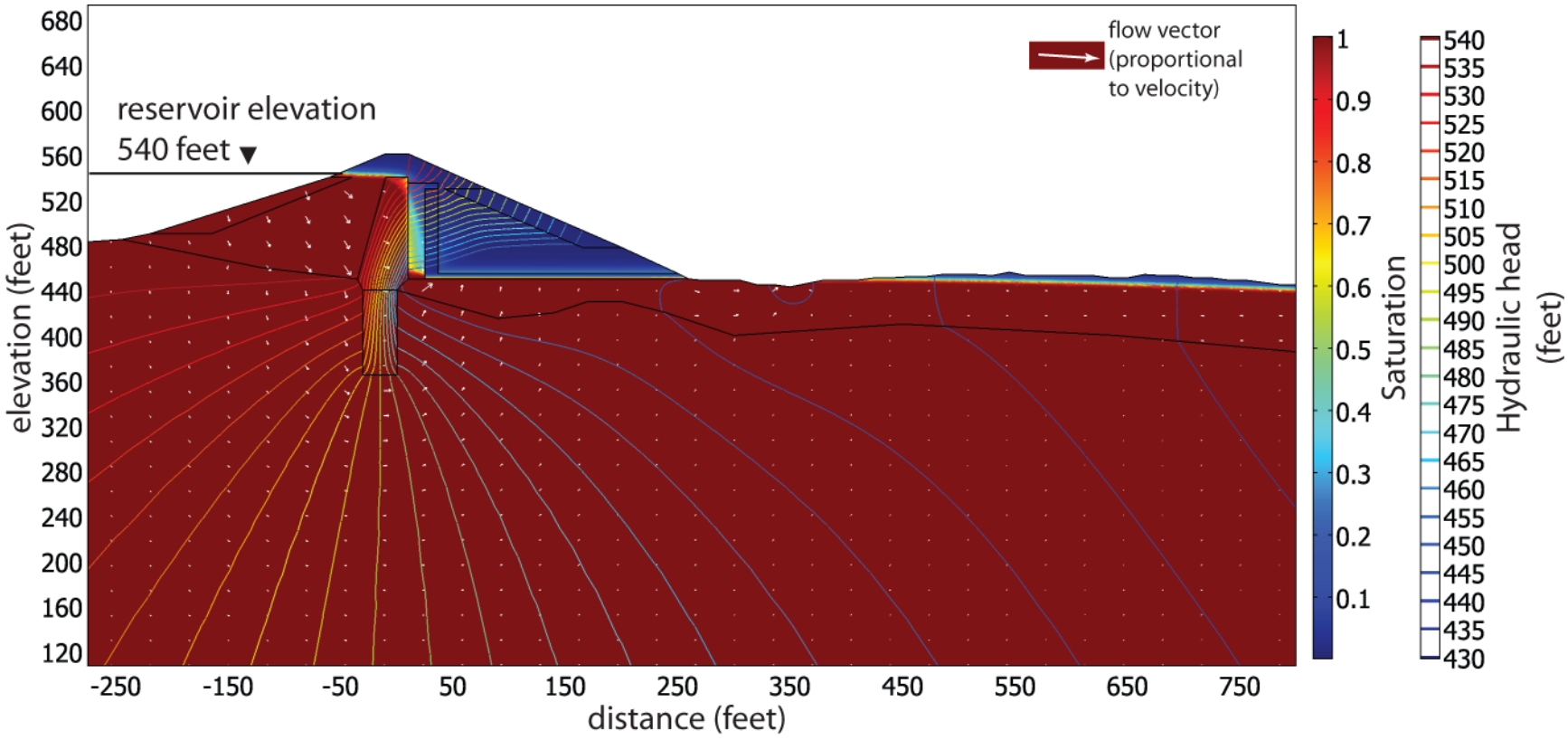

Figure 30. Flow model results for the profile A baseline model with an additional near-surface sediment layer and reservoir elevation of 540 ft (flow scenario 4). Background colors represent the effective saturation, contours indicate hydraulic head (feet), and white arrows show flow directions and relative magnitude.

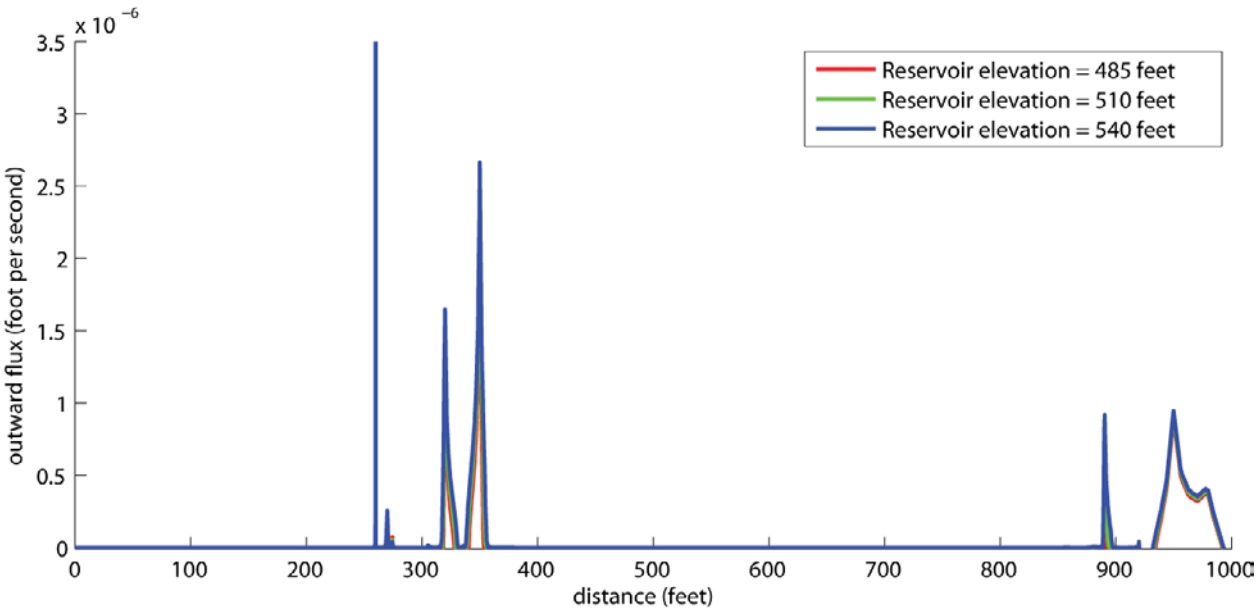

Figure 31. Seepage (feet per second) through the downstream embankment and ground surface as a function of distance for the three different reservoir elevations illustrated in figure 28–30 (flow scenario 4).

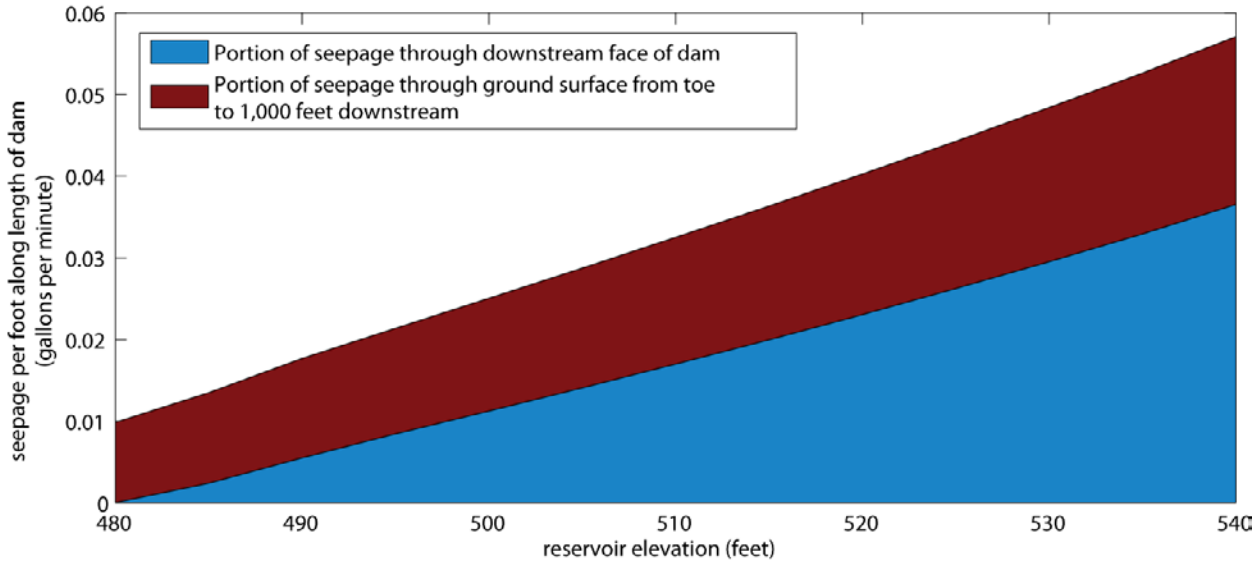

Figure 32. Volumetric flow (gallons per minute) through the downstream embankment (blue) and ground surface (red) per foot along the length of the dam as a function of reservoir elevation for flow scenario 4.

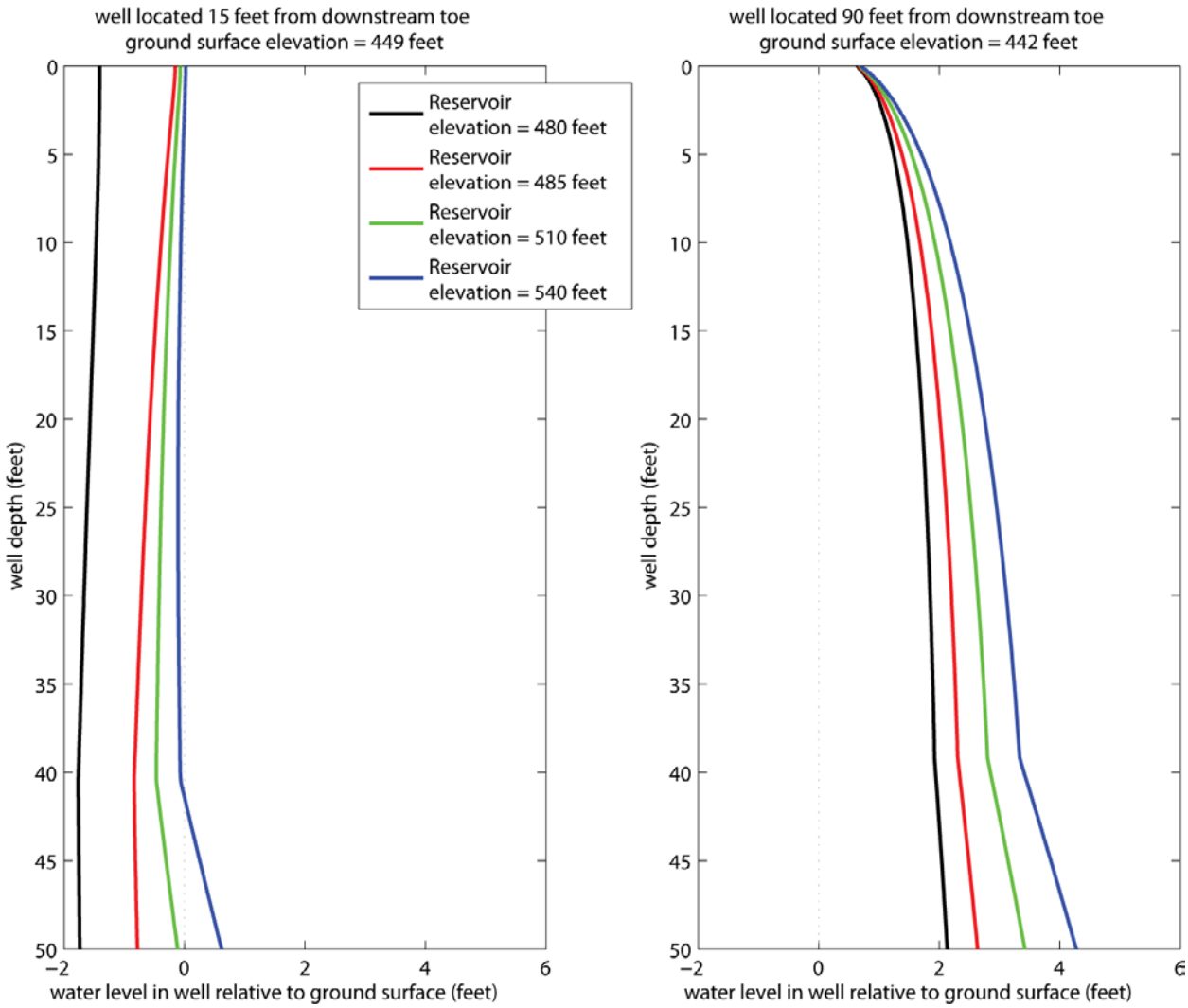

Figure 33. Predicted water levels in observation wells 15 feet (left) and 90 feet (right) from the downstream toe for flow scenario 4. The predicted water level relative to ground surface (positive upwards) is shown for different reservoir elevations and any well depth between 0 and 50 feet.

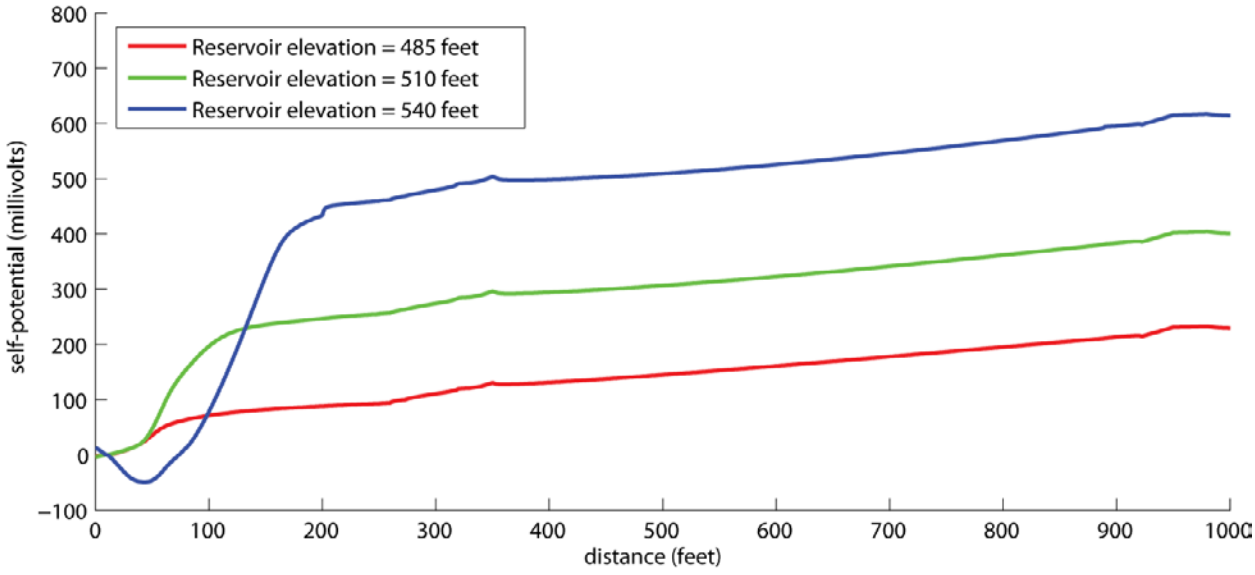

Figure 34. Self-potential (millivolts) values predicted along the downstream embankment and ground surface for the three different reservoir elevations illustrated in figure 28–30 for flow scenario 4.

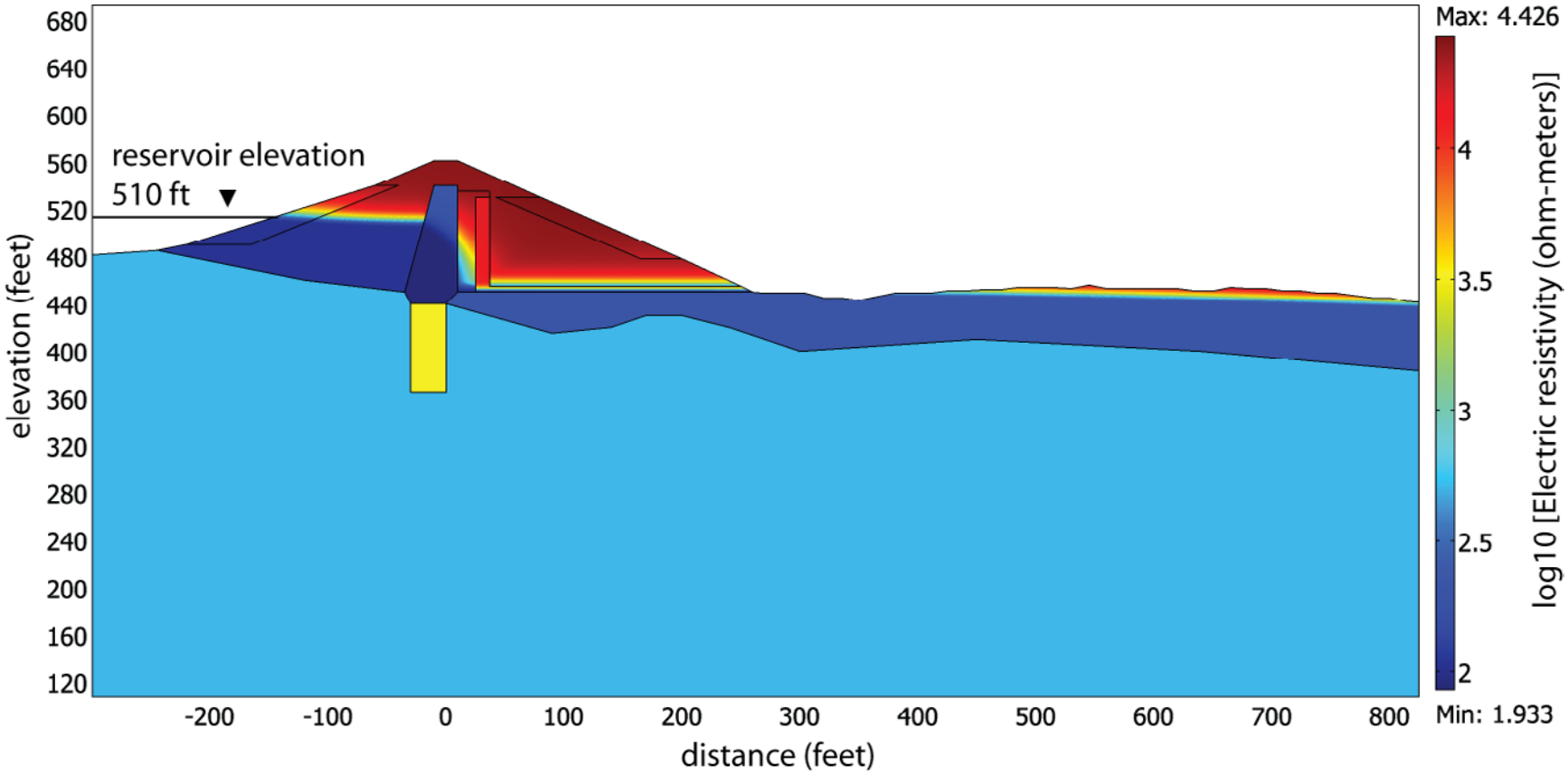

Figure 35. Electrical resistivity (ohm-meters) predicted for flow scenario 4 at a reservoir elevation of 510 feet.

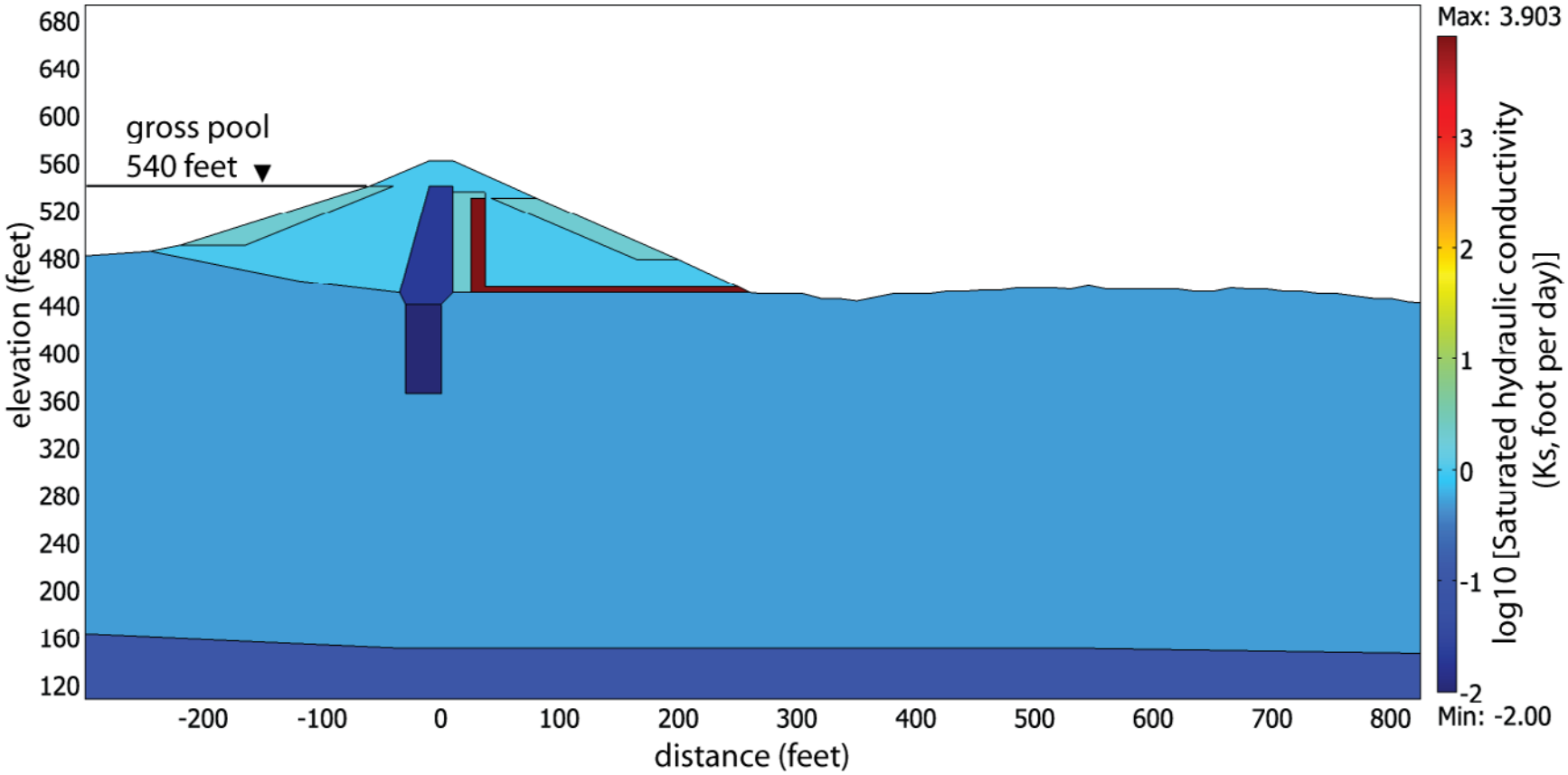

Figure 36. Saturated hydraulic-conductivity values for scenario 5 are identical to scenario 1 (figure 3), with the addition of a higher conductivity channel that extends to several hundred feet depth and connects the upstream and downstream portions of the model.

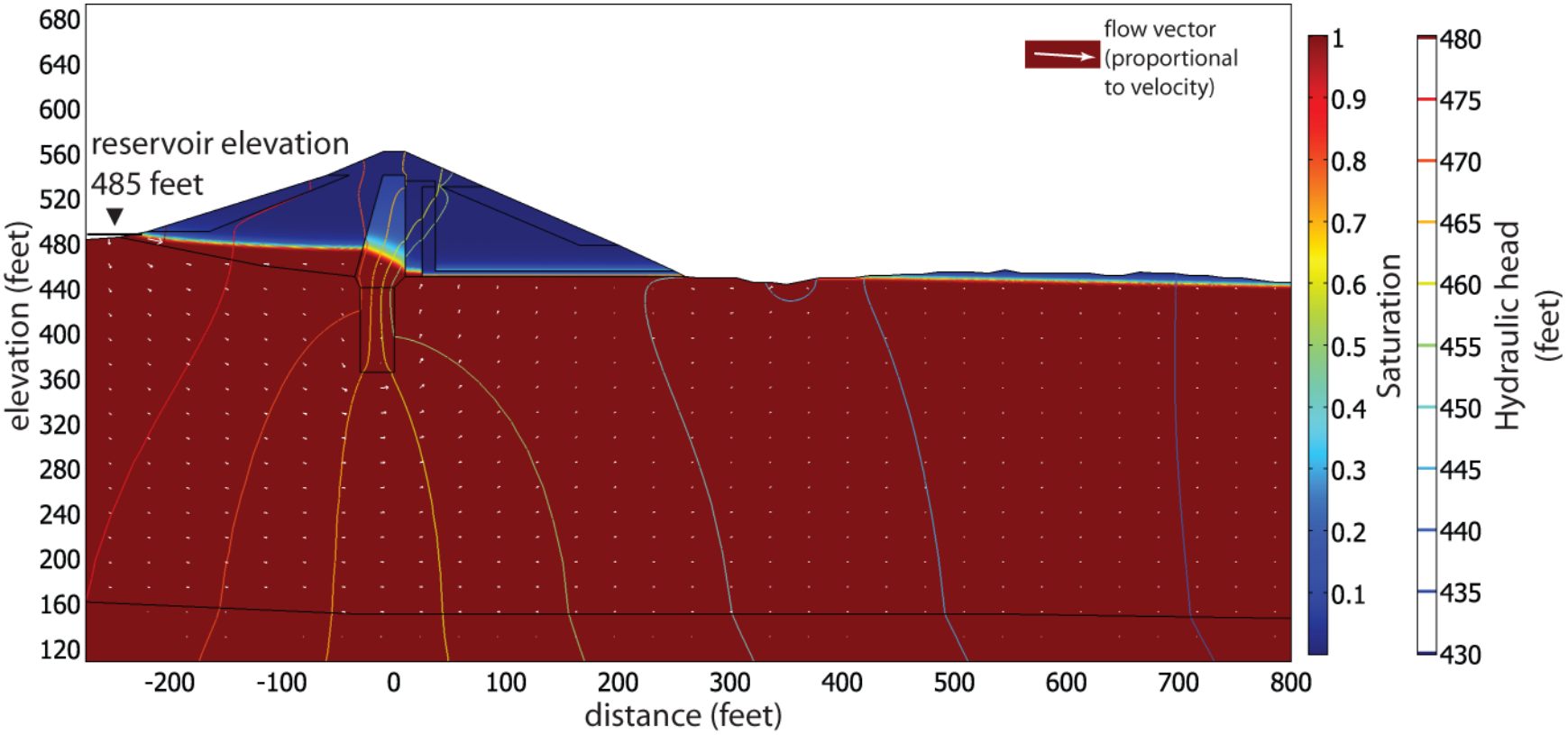

Figure 37. Flow model results for the profile A baseline model with an additional deep sediment channel and reservoir elevation of 485 ft (flow scenario 5). Background colors represent the effective saturation, contours indicate hydraulic head (feet), and white arrows show flow directions and relative magnitude.

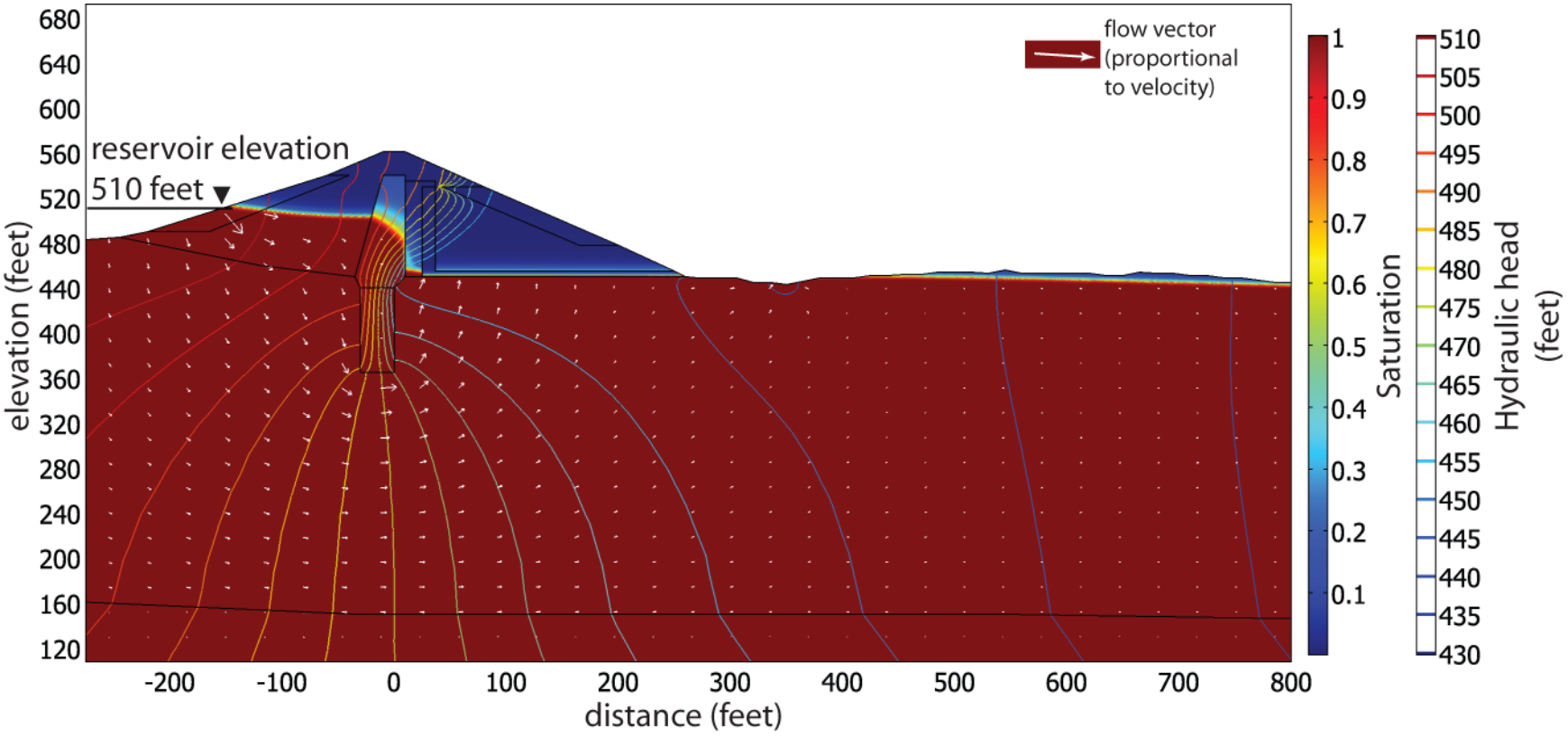

Figure 38. Flow model results for the profile A baseline model with an additional deep sediment channel and reservoir elevation of 510 ft (flow scenario 5). Background colors represent the effective saturation, contours indicate hydraulic head (feet), and white arrows show flow directions and relative magnitude.

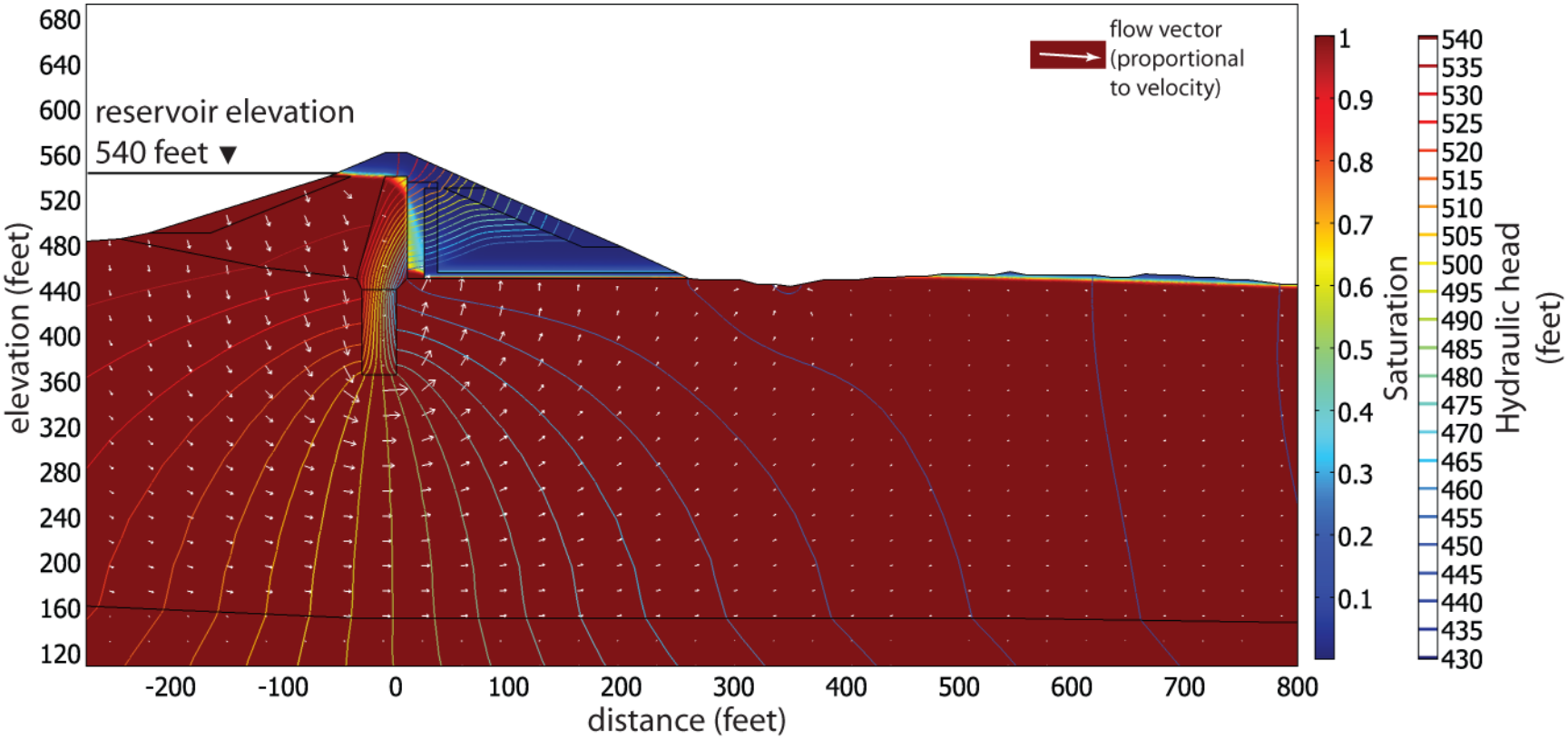

Figure 39. Flow model results for the profile A baseline model with an additional deep sediment channel layer and reservoir elevation of 540 ft (flow scenario 5). Background colors represent the effective saturation, contours indicate hydraulic head (feet), and white arrows show flow directions and relative magnitude.

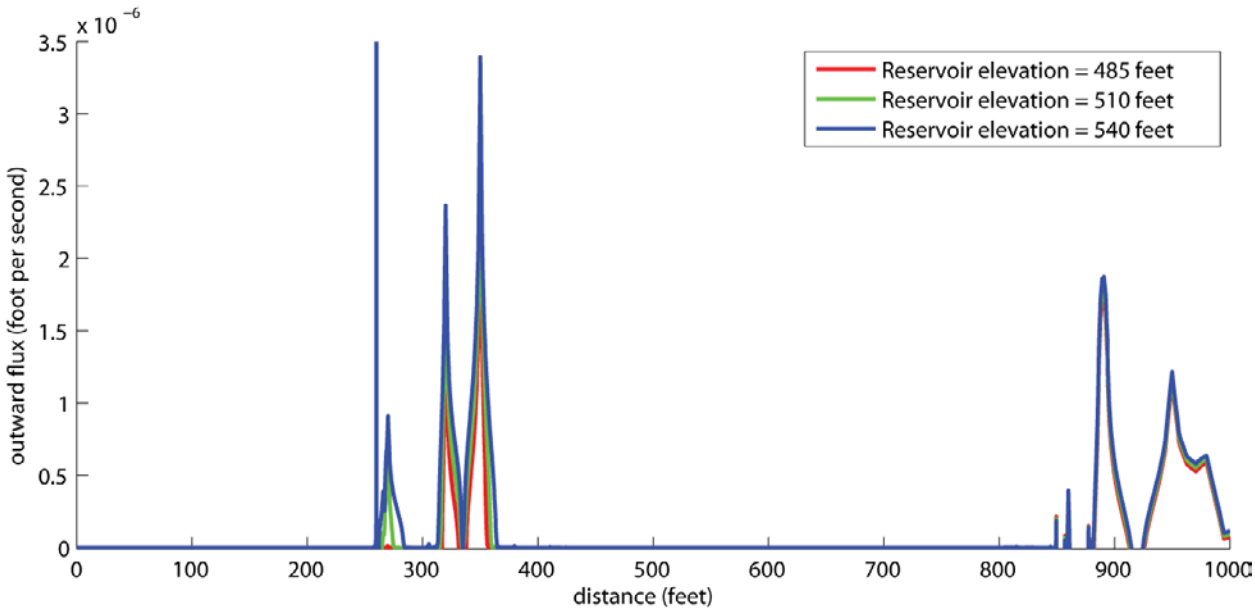

Figure 40. Seepage (feet per second) through the downstream embankment and ground surface as a function of distance for the three different reservoir elevations illustrated in figure 37–39 (flow scenario 5).

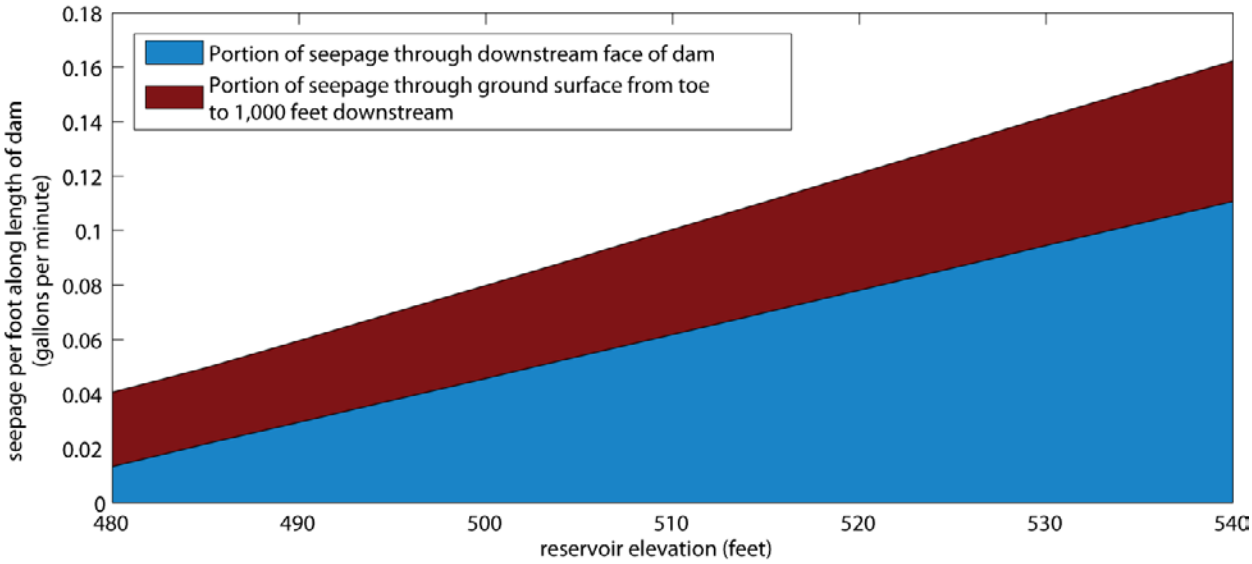

Figure 41. Volumetric flow (gallons per minute) through the downstream embankment (blue) and ground surface (red) per foot along the length of the dam as a function of reservoir elevation for flow scenario 5.

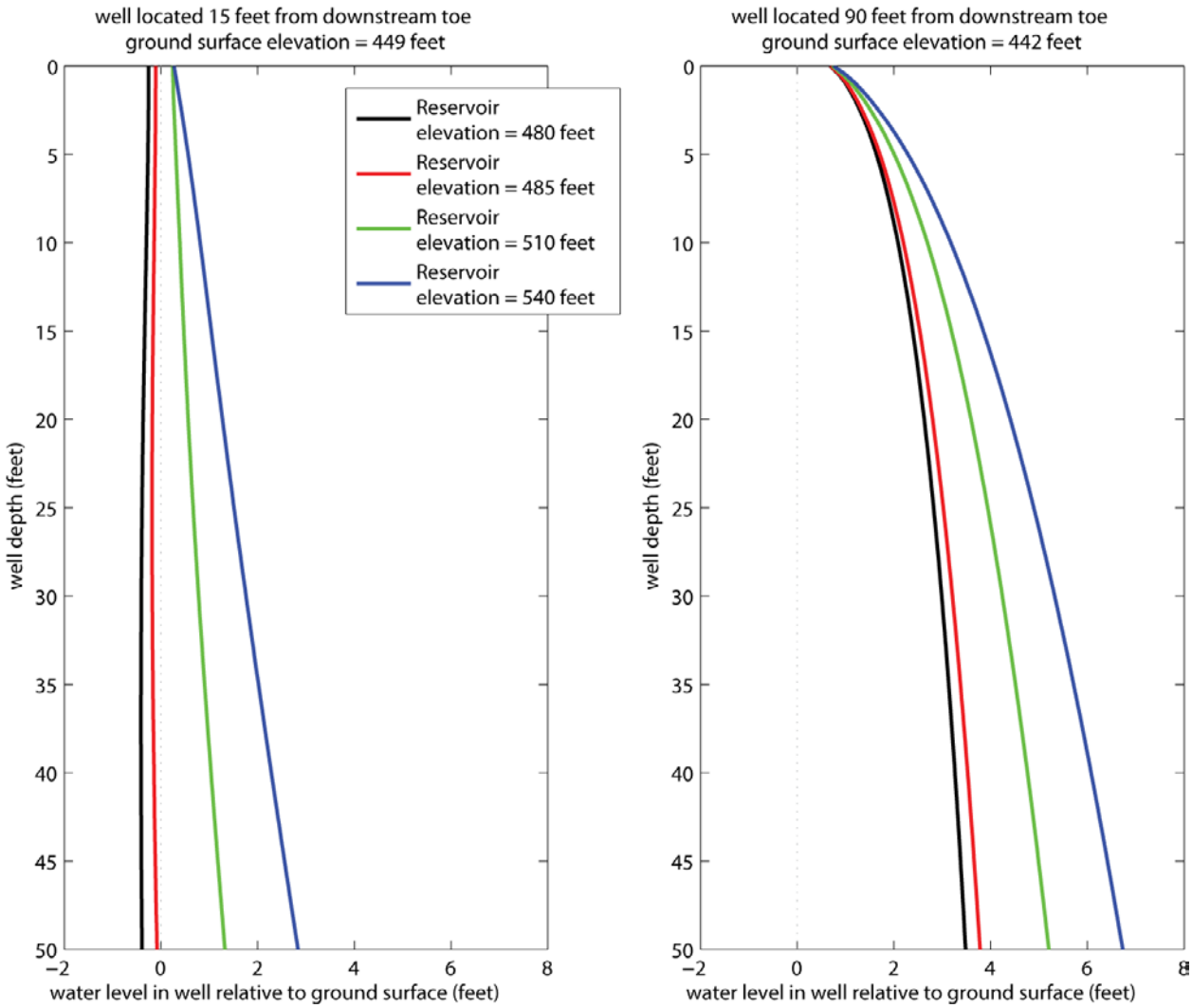

Figure 42. Predicted water levels in observation wells 15 feet (left) and 90 feet (right) from the downstream toe for flow scenario 5. The predicted water level relative to ground surface (positive upwards) is shown for different reservoir elevations and any well depth between 0 and 50 feet.

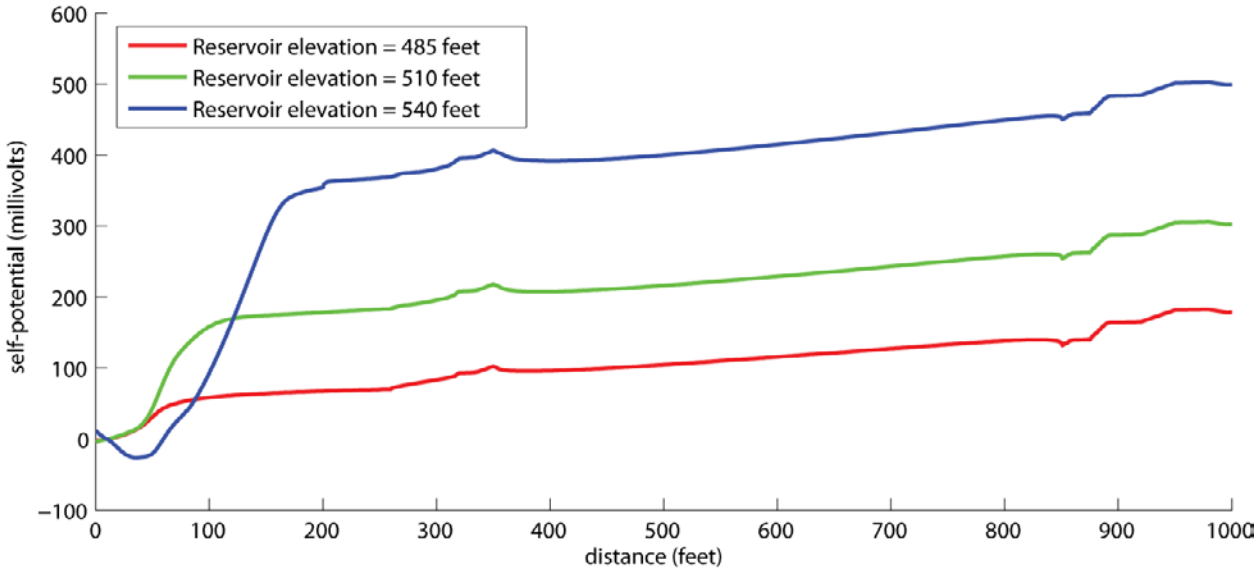

Figure 43. Self-potential (millivolts) values predicted along the downstream embankment and ground surface for the three different reservoir elevations illustrated in figure 37–39 for flow scenario 5.

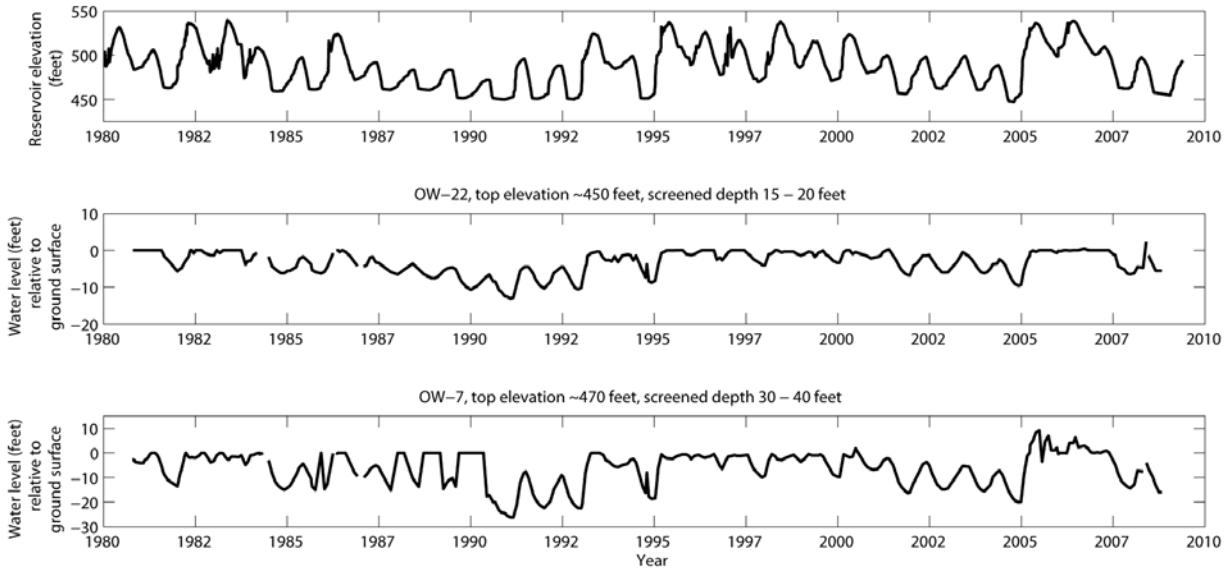

Figure 44. Historical record of reservoir elevation (top) and water levels relative to ground surface (negative values are below ground) for observation wells OW-22 and OW-7.

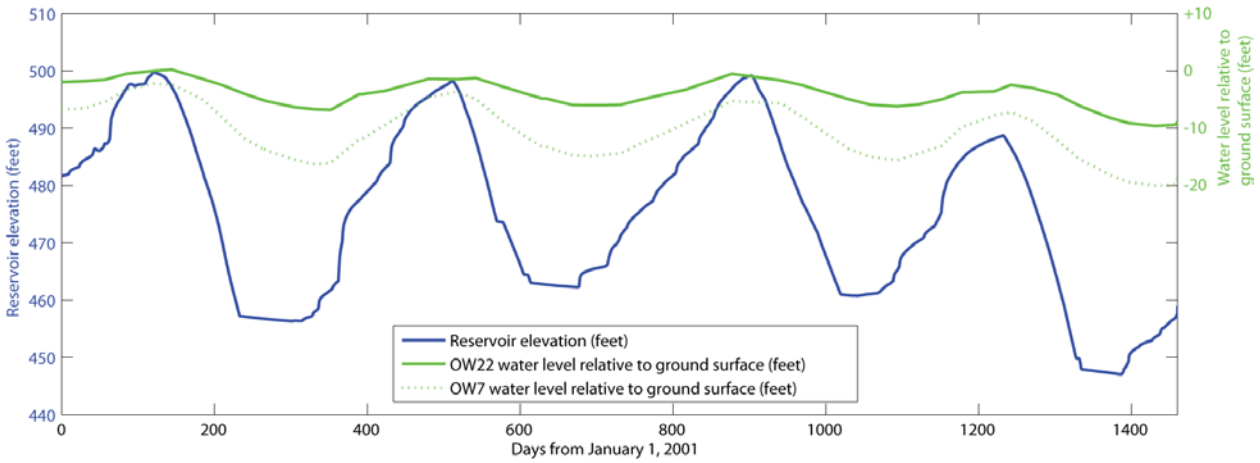

Figure 45. Detailed view of reservoir elevation and observation-well data for OW-22 and OW-7 from 2001–2004.

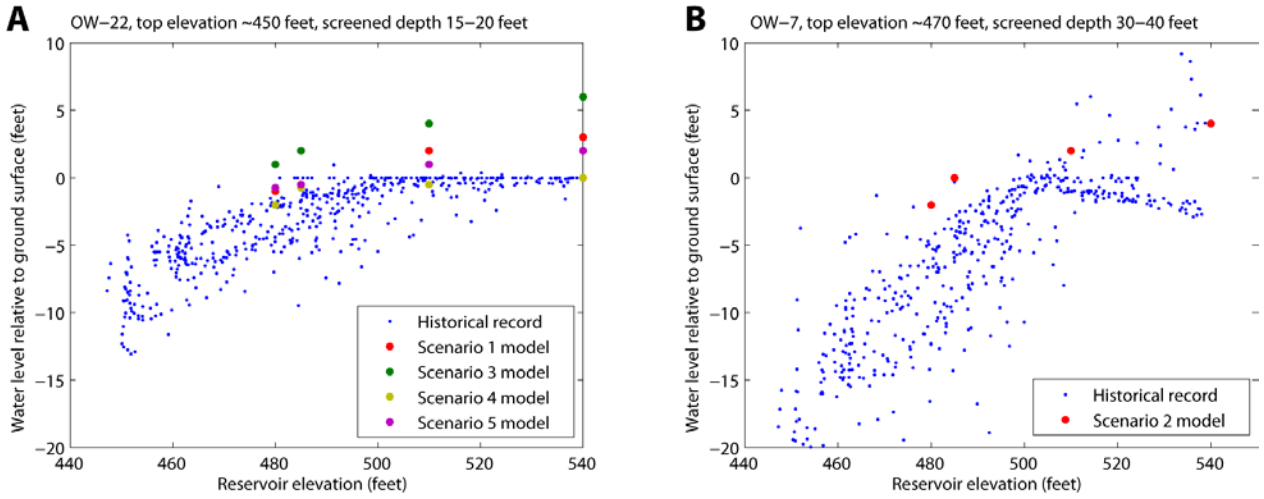

Figure 46. Crossplots of reservoir elevation and observation-well water level data for OW-22 (A) and OW-7 (B), along with model-predicted results from the various flow scenarios in this study. The large number of zero-values and absence of positive water levels in the OW-22 data indicate the inability to record water levels that are higher than the ground surface. In OW-7, above-ground water levels are measured with pressure transducers.

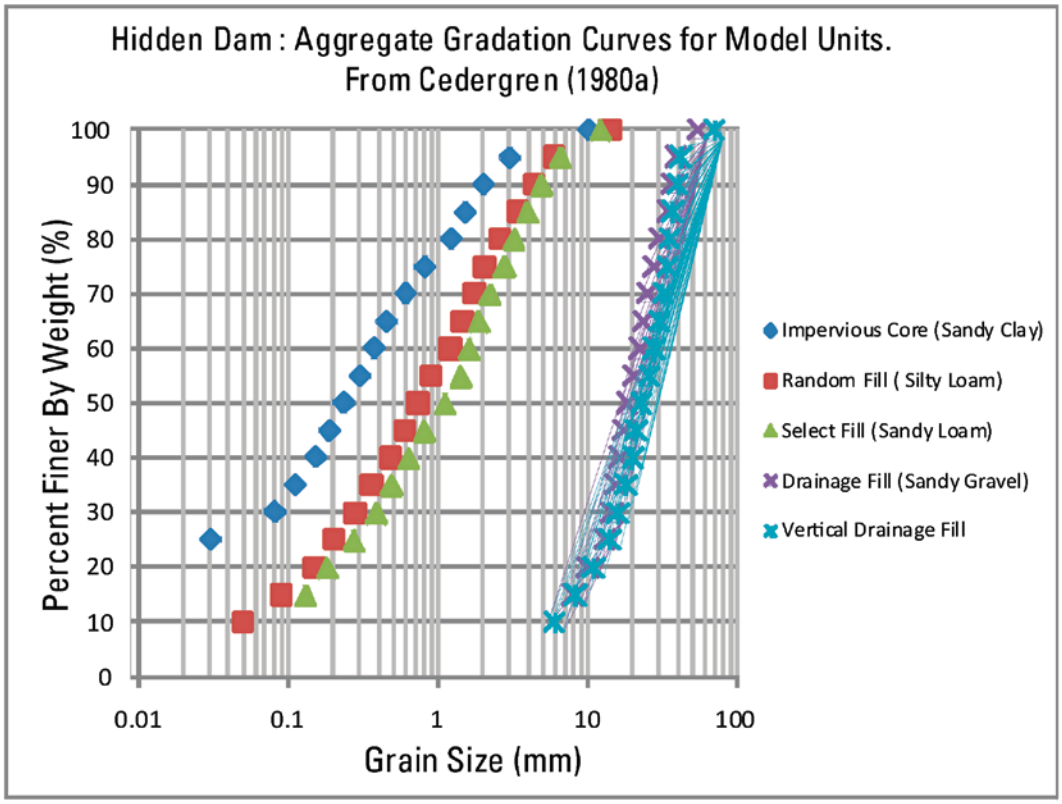

Figure 47. Gradation curves for primary Hidden Dam model units.

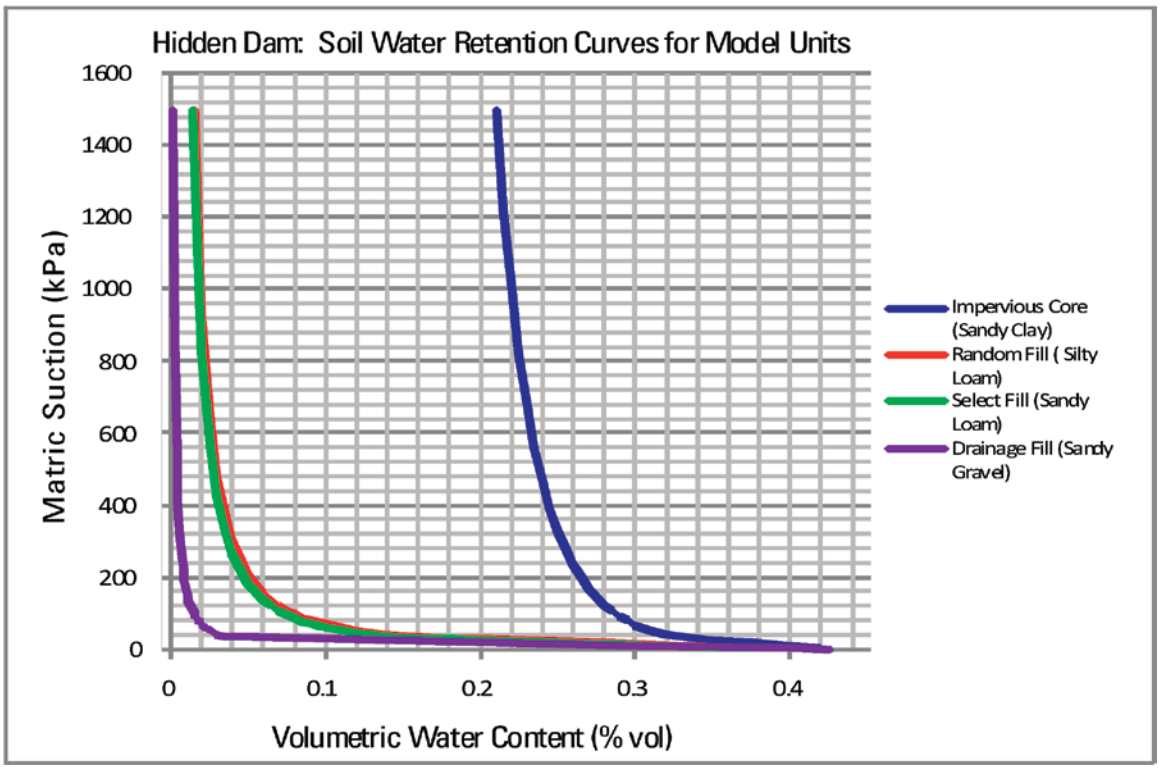

Figure 48. Soil-water retention curves for primary Hidden Dam model units.